
Turbulence Modelling for Smoothed Particle Hydrodynamics

*Report submitted in partial fulfillment of the requirements of the degree of
Master of Technology*

by

K T Prajwal Prathiksh

Roll No. : 180010027

Supervisor:

Prof. Prabhu Ramachandran



Department of Aerospace Engineering
Indian Institute of Technology Bombay

June - October 2022

Declaration of Authorship

I, K T Prajwal Prathiksh, hereby declare that this written submission on "*Turbulence Modelling for Smoothed Particle Hydrodynamics*", represents my ideas in my own words and where others' ideas or words have been included, I have adequately cited and referenced the original sources. I also declare that I have adhered to all principles of academic honesty and integrity and have not misrepresented or fabricated or falsified any idea/data/fact/source in my submission. I understand that any violation of the above will be cause for disciplinary action by the *Indian Institute of Technology Bombay*, and can also evoke penal action from the sources which have thus not been properly cited or from whom proper permission has not been taken when needed.

Date:

October 22, 2022

Student Name: K T Prajwal Prathiksh

Roll No.: 180010027

INDIAN INSTITUTE OF TECHNOLOGY BOMBAY

Abstract

Prof. Prabhu Ramachandran

Master of Technology

Turbulence Modelling for Smoothed Particle Hydrodynamics

by K T Prajwal Prathiksh

Turbulence modelling is a challenging problem, particularly for a Lagrangian method such as Smoothed Particle Hydrodynamics (SPH) which lacks the years of theoretical and practical research that conventional CFD solvers based on FEM/FVM enjoy. However, work based on translating existing Eulerian-based turbulence methods to SPH and Lagrangian-specific models has started making inroads in the general understanding of the topic in an SPH setting. Ultimately, a rigorous and robust model can be devised, which is suitable for a wide variety of 2D and 3D problems.

This project aims to survey and review the state-of-the-art turbulence models that SPH offers and help subsequently provide a comparative analysis detailing the advantages and limitations of these models. It also intends to extend the best-equipped models to robust and accurate SPH schemes and incorporate some of the latest developments in the field of SPH to refine further the machinery required to model turbulence.

Keywords: Fluid Mechanics, Turbulence Modelling, Smoothed Particle Hydrodynamics, Reynolds Averaging, Large Eddy Simulation, Lagrangian Averaging, Coherent Structures

Contents

Declaration of Authorship	I
Abstract	II
Contents	III
List of Figures	V
List of Symbols	VII
1 Introduction	1
1.1 Smoothed Particle Hydrodynamics	2
1.2 Project Motivation & Objectives	2
1.3 Report Structure	3
2 Turbulence Modelling	4
2.1 Viscosity-Based Models	4
2.1.1 Eddy Viscosity Model	4
2.1.2 Generalized Langevin Model	5
2.1.3 mSPH	7
2.2 Large Eddy Simulation-based Models	10
2.2.1 Implicit Pressure Poisson-based Models	10
2.2.2 Explicit Pressure Equation of State-based Models	15
2.3 Lagrangian LES-based Models	23
2.3.1 Extension to EDAC-SPH Scheme	27
2.4 RANS-based k-epsilon Models	27
2.5 LANS-based Models	31
2.6 Miscellaneous Models	33
3 Evaluation of Turbulence Models	35
3.1 Benchmark Problems	35
3.1.1 Taylor-Green Vortex Problem	35
3.1.2 Thin Double-Shear Layer	36
3.1.3 3D Isotropic Turbulence	36
3.1.4 2D Confined and Driven Turbulence	36
3.1.5 Free Surface Flows	36
3.2 Post-Simulation Analysis	37
3.2.1 Energy Spectral Density	37
3.2.2 Lagrangian Coherent Structures	38
4 Conclusion & Future Work	40
A Lagrangian LES Filtering of EDAC	41

Bibliography	43
--------------	----

List of Figures

1.1	A scanned copy of a part of the first page of the 1887 paper by William Thomson, where the word ' <i>turbulence</i> ', as a noun, is first introduced. Reproduced from Schmitt 2017	2
2.1	Turbulent Poiseuille flow in a pipe ($Re = 6.4 \times 10^4$) modelled using the eddy viscosity model. Computed mean velocity profiles after ($t = 1s$) (solid circles), against theory (solid line). Reproduced from VIOLEAU, PICCON, and CHABARD 2002	5
2.2	Turbulent Poiseuille flow in a pipe ($Re = 6.4 \times 10^4$) modelled using the generalised Langevin model. Computed mean velocity profiles after ($t = 1s$) (solid circles), against theory (solid line). Reproduced from VIOLEAU, PICCON, and CHABARD 2002	7
2.3	Velocity vector plot at $t = 2$ (left) and $t = 30$ (right). $Re = \infty$. Reproduced from Adami, X. Y. Hu, and N. A. Adams 2012	8
2.4	Comparison of energy spectra $t = 10$. + and \times denote standard SPH results with quintic spline and MLS interpolation; \circ and \square denote mSPH results with quintic spline and MLS interpolation. Reproduced from Adami, X. Y. Hu, and N. A. Adams 2012	9
2.5	Dissipation rate at $Re = 400$ using DNS (solid line), Smagorinsky model (dashed line), standard SPH (+) and mSPH (\circ). Reproduced from Adami, X. Y. Hu, and N. A. Adams 2012	9
2.6	Dissipation rate at $Re = 3000$ using DNS (solid line), Smagorinsky model (dashed line) and mSPH (\circ). Reproduced from Adami, X. Y. Hu, and N. A. Adams 2012	10
2.7	Time sequences of computational and experimental wave profiles near curtain wall (overtopping). Reproduced from Hitoshi Gotoh, Songdong Shao, and Memita 2004	13
2.8	Experimental and computational wave profiles by SPH and MPS model. Reproduced from Songdong Shao and Hitoshi Gotoh 2005	14
2.9	Cylinder distribution and instantaneous velocity overlapped by velocity vectors. Velocity in m/s , at $t = 20s$. The flow direction is from left to right. Reproduced from Canelas et al. 2016	17
2.10	Vorticity field. Vorticity in Hz, at $t = 20s$. Reproduced from Canelas et al. 2016	18
2.11	FTLE field with negative integration time ($T = -0.4s$) (unstable manifolds - attracting LCS) at $t = 20s$. Reproduced from Canelas et al. 2016	18
2.12	Comparison of quantitative metrics for different particle counts N . (a) & (b) Temporal evolution of the density-weighted averaged kinetic energy. (c) & (d) Temporal evolution of the averaged dissipation rate. Reproduced from Okrashevski et al. 2022	20

2.13 Backward FTLE at the plane $z = \pi$ for $N = 2563$ and $t = 14s$ in the range [11; 14]s. (a) Without explicit SFS model. (b) With the SMAG model. (c) With SIGMA model. (d) With the SMAG-MCG model. Reproduced from Okrashevski et al. 2022	21
2.14 Comparison of quantitative metrics for different $N = 256^3$ runs. (a) & (b) Temporal evolution of the density-weighted averaged kinetic energy. (c) & (d) Temporal evolution of the averaged dissipation rate. Reproduced from Okrashevski et al. 2022	22
2.15 2D freely decaying turbulence ($tU/L = 2$, $Re = 1.25 \times 10^5$). Left: Energy spectrum using DNS-SPH. Right: Energy spectrum using LES-SPH. Reproduced from Di Mascio et al. 2017	25
2.16 3D homogeneous turbulence decay. Comparison between DNS-SPH and LES-SPH simulations ($tU/L = 5$). Left: Particle resolution = 64^3 . Right: particle resolution = 128^3 . Reproduced from Di Mascio et al. 2017	25
2.17 Left: Energy spectrum at ($tU/L = 3$, $Re = 1 \times 10^6$) as predicted by the δ -LES-SPH model and a finite volume scheme. Symbols k_f and k_R indicate the wave numbers of the external forcing and the kernel radius, respectively, while k_λ and k_D are the wave numbers associated with the Taylor and Kolmogorov scales. Right: k field at the same instant. Reproduced from Colagrossi 2021	26
2.18 Left: Time histories of k as predicted by finite volume scheme and the δ -LES-SPH model. Right: Energy spectra. Symbols k_f and k_R denote the wave numbers of the external forcing and the kernel radius, respectively. Reproduced from Colagrossi 2021	26
2.19 Comparisons of computed water surface elevations by SPH (solid lines) with experimental (\circ) and numerical (dotted lines) data of Li et al. (T. Li, Troch, and De Rouck 2004). Reproduced from Songdong Shao 2006	29
2.20 Comparisons between experimental data (left) and numerical results (right) for turbulence intensity (m/s) at $t = 0.6s$ (top panels) and the corresponding vertical cross-sections (lower panels). In the lower panels, solid lines and \circ represent the numerical and experimental results, respectively. Reproduced from Wang and P. L. Liu 2020	30
2.21 Comparisons of numerical and experimental turbulent kinetic energy in x-direction and y-direction. Reproduced from Wang and P. L. Liu 2020	31
3.1 Viscous flow past a circular cylinder at $Re = 105$. Top: Attracting FTLE contour plot from SPH simulation. Bottom: Photo from experiments conducted by Taneda (Taneda 1977) with electrolytic precipitation in water technique for vortex street visualisation. Reproduced from Sun, Colagrossi, et al. 2016	39

List of Symbols

Symbol	Description
\mathbf{a}	Vector Field
$\underline{\mathbf{A}}$	Second-rank Tensor Field
$\underline{\mathbf{I}}$	Identity Tensor
$\hat{\mathbf{e}}_i$	i^{th} Basis
\otimes	Tensor Product
$\frac{\mathrm{D}(\cdot)}{\mathrm{D}t}$	Lagrangian Derivative
$\langle \underline{\mathbf{A}}, \underline{\mathbf{B}} \rangle$	Frobenius Inner Product of $\underline{\mathbf{A}}$ and $\underline{\mathbf{B}}$
$\ \underline{\mathbf{A}}\ _F$	Frobenius Norm of $\underline{\mathbf{A}}$ ($= \sqrt{\langle \underline{\mathbf{A}}, \underline{\mathbf{A}} \rangle}$)
∇^2	Laplacian Operator
$\Delta(\cdot)$	Component-wise Laplacian Operator
$(1 - \alpha^2 \Delta)$	Helmholtz Operator
i	Reference Particle
j	Neighbouring Particle
$(\dots)_i$	Property of i^{th} SPH particle
$(\dots)_j$	Property of j^{th} SPH particle
$(\dots)_{ij}$	$(\dots)_i - (\dots)_j$
n_{dim}	Number of spatial dimensions for a given problem
t	Time
\mathbf{r}	Position = (x, y, z)
\mathbf{v}	Velocity = (v_x, v_y, v_z)
m	Mass
P	Pressure

Table 1 continued from previous page

Symbol	Description
ρ	Density
$(\dots)_0$	Initial Condition ($t = 0$) of Specified Property
Δt	Time Step
Δx	Inter Particle Spacing
$\delta(x)$	Dirac Delta Function
W_h	SPH Interpolating Kernel
h	Kernel Smoothing Length
$W_{h,ij}$	$W(\mathbf{r}_{ij} , h)$
$\nabla_i W_{h,ij}$	$\nabla_i W(\mathbf{r}_{ij}, h) = \frac{\mathbf{r}_{ij}}{ \mathbf{r}_{ij} } \frac{\partial W_{h,ij}}{\partial r_i}$
\mathcal{V}_i	Volume of i^{th} SPH particle
φ_i	Particle Density of i^{th} SPH particle
\mathbf{F}	External Body Force
ν	Kinematic Viscosity
η	Dynamic Viscosity ($= \nu\rho$)
ξ	Machine Epsilon
M_o	Reference Mass
P_o	Reference Pressure
ρ_o	Reference Density
c_s	Speed of Sound
γ	Exponent - Equation of State
$\boldsymbol{\omega}$	Vorticity ($= \nabla \times \mathbf{v}$)
ν_t	Turbulent Eddy Viscosity
\underline{S}	Strain-Rate Tensor ($= [1/2][\nabla \mathbf{v} + \nabla \mathbf{v}^T]$)
\underline{R}	Rate of Rotation Tensor ($= [1/2][\nabla \mathbf{v} - \nabla \mathbf{v}^T]$)
ϵ	Turbulent Dissipation Rate
k	Turbulent Kinetic Energy

Table 1 continued from previous page

Symbol	Description
$\underline{\tau}$	Stress Tensor
C_s	Smagorinsky Constant
u_{max}	Maximum Particle Velocity
ε	Smoothing Parameter (XSPH)
k	Wave Number

1 Introduction

Turbulence is the most important unsolved problem of classical physics.

Richard Feynman

Turbulent flows have long been a phenomenon that is surprisingly easy to detect and observe in the natural world but unmistakably challenging to understand and model in sufficient detail, unlike other problems in classical physics. The fundamental aspects of turbulent flow consisting of eddies of various length scales had long been observed, as recorded by Leonardo Da Vinci's 16th century diagrams of water flow in streams and channels from the (A. Colagrossi et al. 2021). It took the work of Osborne Reynolds on his averaging of the Navier-Stokes equations and William Thomson's (Lord Kelvin) work on flow along an inclined plane (see Fig. 1.1) for *turbulence* to enter the parlance of the larger scientific community. This allowed turbulence to be recognised as a new subfield of fluid mechanics.

However, further strides in the field have remained arduous despite the Navier-Stokes (NS) equations being written down in the early 19th century. There is consensus that this remarkable failure of some of the greatest scientific minds in providing an intricate understanding of turbulence points to an inadequacy of the mathematical tools we have at our disposal. Even the current machinery cannot deal with the strong non-linearity of the equations coupled with the characteristic tendency of flows to degenerate into some form of instability.

Turbulence is caused by excessive kinetic energy in parts of a fluid flow that can overcome the damping effect of the fluid's viscosity. Its onset can be predicted by the dimensionless Reynolds number, which is the ratio of kinetic energy to viscous damping in a fluid flow.

The criteria for defining a flow as turbulent are varied and ambiguous since there is no explicit definition for it. However, the most often used criteria for qualifying a flow as turbulent is given below (Sagaut 2002):

- random character of the spatial and temporal fluctuations of the velocities, which reflect the existence of finite characteristic scales of statistical correlation;
- velocity field is three-dimensional and rotational;
- various modes are strongly coupled, which is reflected in the non-linearity of the NS equations;
- large mixing capacity due to the agitation induced by the various scales;
- chaotic character of the solution, which exhibits a powerful dependency on the initial condition and boundary conditions.

[272]

XXXIV. Stability of Motion (continued from the May, June, and August Numbers).—Broad River flowing down an Inclined Plane Bed. By Sir WILLIAM THOMSON, F.R.S.*

41. CONSIDER now the second of the two cases referred to in § 27—that is to say, the case of water on an inclined plane bottom, under a fixed parallel plane cover (ice, for example), both planes infinite in all directions and gravity everywhere uniform. We shall include, as a sub-case, the icy cover moving with the water in contact with it, which is particularly interesting, because, as it annuls tangential force at the upper surface, it is, for the steady motion, the same case as that of a broad open river flowing uniformly over a perfectly smooth inclined plane bed. It is not the same, except when the motion is steadily laminar, the difference being that the surface is kept rigorously plane, but not free from tangential force, by a rigid cover, while the open surface is kept almost but not quite rigorously plane by gravity, and rigorously free from tangential force. But, provided the bottom is smooth, the smallness of the dimples and little round hollows which we see on the surface, produced by turbulence (when the motion is turbulent), seems to prove that the motion must be very nearly the same as it would be if the upper surface were kept rigorously plane, and free from tangential force.

Figure 1.1: A scanned copy of a part of the first page of the 1887 paper by William Thomson, where the word ‘turbulence’, as a noun, is first introduced. Reproduced from Schmitt 2017

1.1 Smoothed Particle Hydrodynamics

Smoothed particle hydrodynamics (SPH) is a technique for problem-solving in *Computational Continuum Dynamics* (CCD). This technique approximates numerical solutions of the equations of fluid dynamics by replacing the fluid with a set of particles. The equations of motion and properties of these particles are determined from the continuum equations of fluid dynamics. They are subsequently discretised based on the particles’ interpolant data. The interpolant can be constructed using analytical functions, and spatial derivatives of the interpolated quantities can then be found using ordinary calculus. There is no need to use a grid, and the description of free surfaces, however complicated, is trivial.

Therefore, this *Lagrangian* based particle formulation uses no background spatial mesh. Since there is no mesh to distort, the method can handle large deformations in a pure Lagrangian frame. Thus, material interfaces can be modelled naturally, and complex constitutive behaviour can be implemented relatively quickly. This allows SPH to have diverse and fascinating applications in various domains that extend beyond the astrophysical and cosmological problems it was initially designed to tackle.

1.2 Project Motivation & Objectives

Despite the success of SPH in simulating transient flows, a robust or rigorous model of turbulence does not seem to exist. Some of the models in use cannot be generalised to a wide variety of turbulence-based problems or scaled to 3D-flows. This limits SPH’s applicability in turbulent flows where conventional FEM/FVM-based CFD solvers have the upper hand, owing to their sophisticated models.

This project aims to survey and review the current state of the art regarding turbulence modelling in SPH and subsequently provide a framework to help establish the advantages and limitations of such models, using a comparative analysis between the major class of models. After that, it is intended to extend the most well-equipped models to robust and accurate SPH schemes (which might not have been the case in the author/s original work) for bounded flows specifically. Such an exercise is expected to either improve the original model or expose any underlying limitations in its assumptions or discretisation.

1.3 Report Structure

The report is structured to present the turbulence models developed for SPH in [Chapter 2](#). Here, the models have been categorised by the fundamental ideas on which they were based. Subsequently, research on analysing turbulence through standard benchmarks problems and methods of quantifying turbulence data is presented in [Chapter 3](#). Finally, the project conclusion and future work for Stage - II of the Dual Degree Project are presented in [Chapter 4](#).

2 Turbulence Modelling

2.1 Viscosity-Based Models

Violeau et al. (VIOLEAU, PICCON, and CHABARD 2002) were amongst the early pioneers who tried to incorporate a turbulence model in SPH. They came up with two techniques to tackle the problem of turbulence in a Lagrangian framework, which so far had been neglected till then in research, namely, the eddy viscosity model and a generalised Langevin model. For each of their techniques, they considered the following equation of state Eq. 2.1, continuity equation Eq. 2.2 and momentum equation Eq. 2.3, based on the work of (J. J. Monaghan 1992):

$$P_i = B \left[\left(\frac{\rho_i}{\rho_o} \right)^\gamma - 1 \right] , \quad B = \frac{\rho_o c_s^2}{\gamma} \quad (2.1)$$

Where, (P, ρ) denotes pressure and density respectively. $(\dots)_i$ denotes the property of the i^{th} SPH particle, $(\dots)_o$ denotes the reference quantities, and (c_s) denotes the speed of sound.

$$\frac{D\rho_i}{Dt} = \sum_j m_j \mathbf{v}_{ij} \cdot \nabla_i W_{h,ij} \quad (2.2)$$

Where $\left[\frac{D(\cdot)}{Dt} \right]$ denotes the Lagrangian derivative, and (m, \mathbf{v}) represent the mass and velocity respectively. Here we adopt the nomenclature of $(\dots)_{ij}$ to denote the difference of a specified property between the i^{th} and j^{th} SPH particle $[(\dots)_i - (\dots)_j]$, and $(\nabla_i W_{h,ij})$ denotes $[\nabla_i W(\mathbf{r}_{ij}, h) = \frac{\mathbf{r}_{ij}}{|\mathbf{r}_{ij}|} \frac{\partial W_{h,ij}}{\partial r_i}]$, where (h) is the kernel smoothing length.

$$\frac{D\mathbf{v}_i}{Dt} = - \sum_j m_j \left(\frac{P_i}{\rho_i^2} + \frac{P_j}{\rho_j^2} + \Pi_{ij} \right) \nabla_i W_{h,ij} + \mathbf{F}_i \quad (2.3)$$

Where (\mathbf{F}) is the external body force, and the viscous term (Π) is defined as:

$$\Pi_{ij} = - \frac{16\nu}{\rho_i + \rho_j} \frac{\mathbf{v}_{ij} \cdot \mathbf{r}_{ij}}{|\mathbf{r}_{ij}|^2 + \xi^2} \quad (2.4)$$

Here (ν) is the kinematic viscosity, and (ξ) is the machine epsilon.

2.1.1 Eddy Viscosity Model

The eddy viscosity model was devised as a first-order closure model, which consisted of a relationship between the Reynolds stress tensor and the mean velocity gradients. Therefore, the momentum equation is similar to the equation in Eq. 2.3, except that the kinematic viscosity is replaced by the eddy viscosity (ν_t), and the velocities are Reynolds-averaged. In the SPH formalism, the diffusion term occurring is therefore defined as given in Eq. 2.5, with the eddy viscosity defined according to

Eq. 2.6.

$$\tilde{\Pi}_{ij} = -8 \frac{\nu_{t,i} + \nu_{t,j}}{\rho_i + \rho_j} \frac{\langle \mathbf{v} \rangle_{ij} \cdot \mathbf{r}_{ij}}{|\mathbf{r}_{ij}|^2 + \xi^2} \quad (2.5)$$

$$\nu_t = L_m^2 \|\underline{S}\|_F = L_m^2 \sqrt{\langle \underline{S}, \underline{S} \rangle} \quad (2.6)$$

Where $\langle \mathbf{v} \rangle$ is Reynolds-averaged velocity, L_m refers to the mixing length scales, and (\underline{S}) is the strain-rate tensor ($= [1/2][\nabla \mathbf{v} + \nabla \mathbf{v}^T]$), where we adopt the nomenclature of (\underline{A}) to represent a second-rank tensor field. Also, here $(\langle \underline{A}, \underline{B} \rangle)$ denotes the Frobenius inner product of \underline{A} and \underline{B} , and $(\|\underline{A}\|_F)$ denotes the Frobenius norm of \underline{A} ($= \sqrt{\langle \underline{A}, \underline{A} \rangle}$). The SPH formulation for the mean velocity gradients are given in Eq. 2.7.

$$\nabla \langle \mathbf{v} \rangle_i = -\frac{1}{\rho_i} \sum_j m_j \langle \mathbf{v} \rangle_{ij} \otimes \nabla_i W_{h,ij} \quad (2.7)$$

Where (\otimes) denotes the tensor product.

On simulating Poiseuille flow for a high Reynolds number case, the authors could show that the velocity profile showed only a slight discrepancy with theory, with the expected log-law profile near the walls Fig. 2.1. This indicated that the model is appropriate for turbulent mixing problems or for cases involving spatially-varying viscosity while restricted to shear flows.

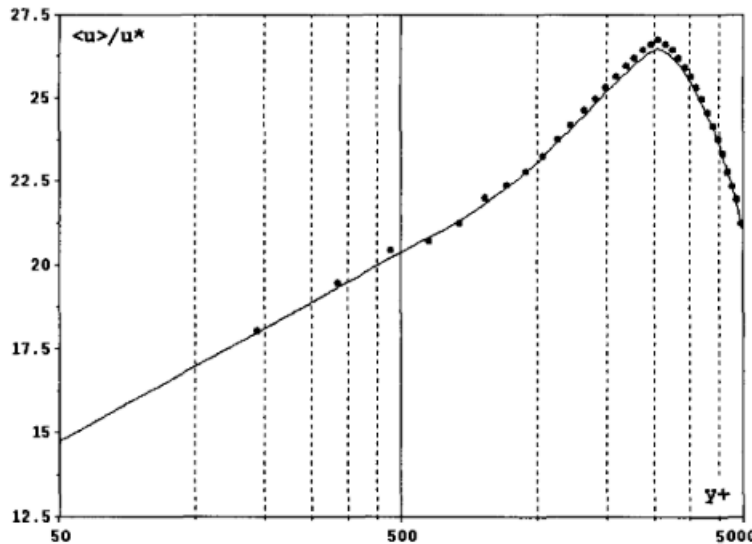


Figure 2.1: Turbulent Poiseuille flow in a pipe ($Re = 6.4 \times 10^4$) modelled using the eddy viscosity model. Computed mean velocity profiles after ($t = 1s$) (solid circles), against theory (solid line). Reproduced from VIOLEAU, PICCON, and CHABARD 2002

2.1.2 Generalized Langevin Model

Violeau et al. (VIOLEAU, PICCON, and CHABARD 2002) also considered a stochastic approach, where the main idea is built on the concept of prescribing particle velocities as a random process, with properties fulfilling the theoretical turbulence hypotheses (S. Pope 1994). Hence, came about the Generalised Langevin model (GLM),

where the particle acceleration is defined as:

$$d\mathbf{v} = -\frac{1}{\rho} \nabla \langle P \rangle + \underline{\mathbf{G}}(\mathbf{v} - \langle \mathbf{v} \rangle) dt + \sqrt{C_0 \epsilon dt} \vec{\xi} \quad (2.8)$$

Where $\vec{\xi}$ is a random vector statistically non-correlated with velocities. The closure for this model was defined by specifying $\underline{\mathbf{G}}$ as:

$$\underline{\mathbf{G}} = \frac{1}{2} C_1 \frac{\epsilon}{k} \mathbf{I} + C_2 \nabla \langle \mathbf{v} \rangle \quad (2.9)$$

Where (k) is the turbulent kinetic energy, (ϵ) the dissipation rate, and (C_i) being constants - ($C_1 = 1.8, C_2 = 0.6$). (\mathbf{I}), here, denotes the identity tensor. By modelling turbulence as GLM in SPH, the momentum equation derived was given by:

$$\frac{D \mathbf{v}_i}{Dt} = - \sum_j m_j \left(\frac{\langle P \rangle_i}{\rho_i^2} + \frac{\langle P \rangle_j}{\rho_j^2} \right) \nabla_i W_{h,ij} - \frac{1}{2} C_1 \frac{\epsilon_i}{k_i} \mathbf{v}'_i + C_2 \nabla \langle \mathbf{v} \rangle_i \cdot \mathbf{v}'_i + \sqrt{\frac{C_0 \epsilon_i}{\delta t}} \vec{\xi}_i \quad (2.10)$$

$$\langle \mathbf{v} \rangle = \sum_j \frac{m_j}{\rho_j} \mathbf{u}_j W_h(\mathbf{r}_j) \quad (2.11)$$

Where the fluctuations are defined as $\mathbf{v}' = \mathbf{v} - \langle \mathbf{v} \rangle$, and the local values of turbulent kinetic energy and dissipation rate are:

$$\epsilon_i = 2\nu_{t,i} + \|\underline{\mathbf{S}}_i\|_F^2 \quad (2.12)$$

$$k_i = \frac{\epsilon_i \nu_{t,i}}{C_\mu} \quad , \quad C_\mu = 0.009 \quad (2.13)$$

It is to be noted that the authors did not estimate the dissipation rate through the proper velocity gradients since the fluctuations of random velocities do not reproduce the small eddies. The same test case as mentioned in Sec. 2.1.1 was considered for the performance of GLM. The authors observed large fluctuations. They attributed the discrepancy to the mean operator being redefined as given by Eq. 2.11 instead of being a Reynolds average. In fact, by redefining the mean operator in such a fashion, they appeared to have constructed a rudimentary LES filter. As observed in Fig. 2.2, the fluctuations have an order of magnitude of $k^{1/2}$. However, as claimed by the authors, unlike the eddy viscosity model, the GLM method can be used for different flows instead of being restricted to only shear flows.

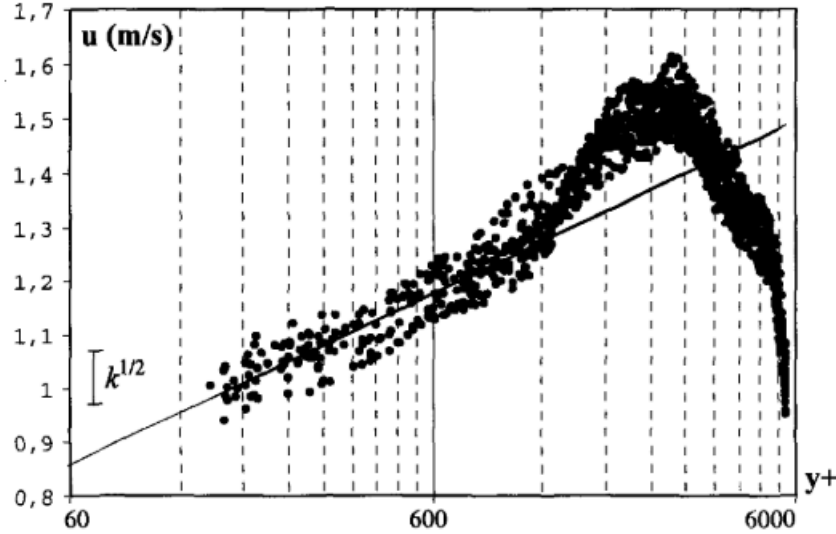


Figure 2.2: Turbulent Poiseuille flow in a pipe ($Re = 6.4 \times 10^4$) modelled using the generalised Langevin model. Computed mean velocity profiles after ($t = 1s$) (solid circles), against theory (solid line).
Reproduced from VIOLEAU, PICCON, and CHABARD 2002

2.1.3 mSPH

Adami et al. (Adami, X. Y. Hu, and N. A. Adams 2012) devised a model built on their observation of SPH simulations, wherein the absence of viscosity in typical SPH formulations produced purely noisy particle motion. At finite viscosities, the method would over-predict dissipation. Hence to counter this, they essentially “modified” (hence the name: Modified SPH [mSPH]) the momentum equation and the equation of state to advect the particles in order to homogenise the particle distribution, in turn stabilising the numerical scheme. They were also able to reduce the artificial dissipation in transitional flows.

The authors considered summation density (Eq. 2.15), which is a function of the volume of the respective SPH particle as given by Eq. 2.14, as opposed to evolving density through the continuity equation (Xiang Yu Hu and Nikolaus A Adams 2006). The modified equation of state as given by Eq. 2.16, is equivalent to the classical SPH equation-of-state with $\gamma = 1$.

$$\mathcal{V}_i = \frac{1}{\sum_j W_{h,ij}} \quad (2.14)$$

$$\rho_i = \frac{m_i}{\mathcal{V}_i} = m_i \sum_j W_{h,ij} \quad (2.15)$$

$$P_i = c_s^2 (\rho_i - \rho_o) \quad (2.16)$$

Where (\mathcal{V}) represents the volume of a particle.

The momentum equation, which provides the acceleration of the particle, is a function of just the gradient and viscous shear forces as given by Eq. 2.17. The corresponding SPH formulation was derived as given by Eq. 2.18, which built on the earlier work of Hu and Adams (X. Hu and Nikolaus A Adams 2007).

$$\frac{D\mathbf{v}}{Dt} = -\frac{1}{\rho} \nabla P + \nu \Delta(\mathbf{v}) + \mathbf{F} \quad (2.17)$$

$$\frac{D\mathbf{v}_i}{Dt} = -\frac{1}{m_i} \sum_j (\mathcal{V}_i^2 + \mathcal{V}_j^2) \frac{P_i \rho_j + P_j \rho_i}{\rho_i + \rho_j} \nabla_i W_{h,ij} - \frac{\eta}{m_i} \sum_j (\mathcal{V}_i^2 + \mathcal{V}_j^2) \frac{\mathbf{v}_{ij}}{|\mathbf{r}_{ij}|} \nabla_i W_{h,ij} + \mathbf{F}_i \quad (2.18)$$

Where $[\Delta(\cdot)]$ denotes the component-wise Laplacian operator, and (η) is the dynamic viscosity.

This scheme takes advantage of the regularisation of the particle motion stemming from the additional background pressure ($P_o = \rho_o c_s^2$). The additional force exerted by the background pressure counteracts non-homogeneous particle distributions, therein reducing numerical dissipation.

The authors estimated the energy spectra of the flow simulations in order to analyse the results of their test cases, using first and second-order moving-least-squares (MLS) method (GOSSLER 2001) and its subsequent Fourier transform (Frigo and Johnson 2005). Their first test case, the 2D variant of the Taylor-Green Vortex (TGV) problem, involved 8×8 counter-rotating vortices, requiring 64^2 particles. They considered the viscosity to be zero. As seen in the time evolution of the

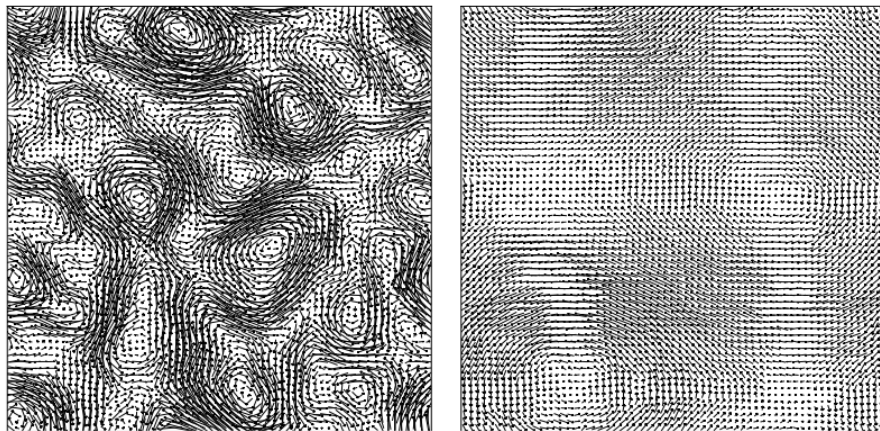


Figure 2.3: Velocity vector plot at $t = 2$ (left) and $t = 30$ (right).
 $Re = \infty$. Reproduced from Adami, X. Y. Hu, and N. A. Adams 2012

The time evolution of the velocity field is given in Fig. 2.3, where it can be observed that the 2D turbulence is characterised by merging and pairing of small vortices. The energy spectra given in Fig. 2.4 show that at low wave numbers, both interpolation schemes give the same results, but at high wave numbers, the results differ. The energy spectrum of the standard SPH has a linear slope of magnitude $m = 1$ in a log-log scale equivalent to a purely noisy velocity field. Theoretically, however, 2D turbulence has an energy cascade with a slope of $m = -3$ in the inertial range, which is reasonably predicted using mSPH.

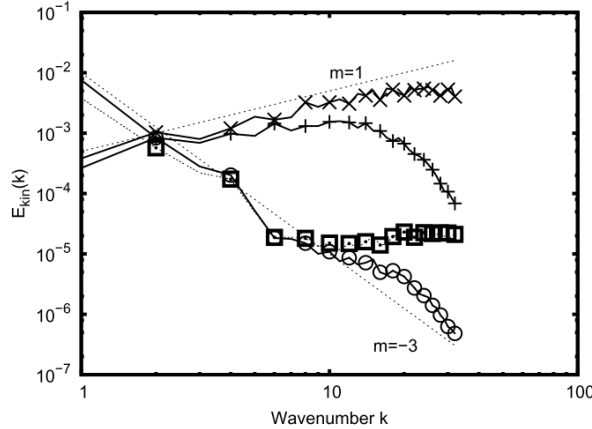


Figure 2.4: Comparison of energy spectra $t = 10$. + and \times denote standard SPH results with quintic spline and MLS interpolation; \circ and \square denote mSPH results with quintic spline and MLS interpolation. Reproduced from Adami, X. Y. Hu, and N. A. Adams 2012

The second test case employed by the authors was that of the 3D TGV problem requiring 64^3 particles for a wide range of Reynolds numbers. The dissipation rate of the flow simulations are shown in Fig. 2.5 and Fig. 2.6. It can be observed that the standard SPH is unable to simulate transitional flows due to excessive dissipation. In contrast, mSPH can reproduce the dissipation rate reasonably well. This implies that the corrected particle transport velocity is an analogous eddy-viscosity model on scales below the numerical resolution.

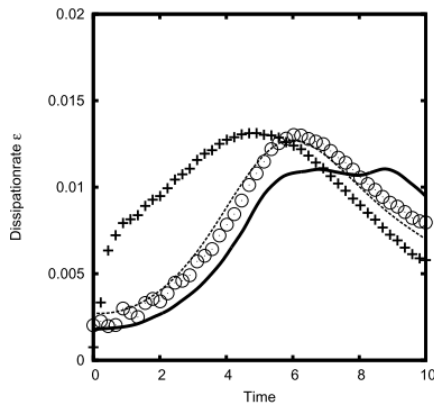


Figure 2.5: Dissipation rate at $Re = 400$ using DNS (solid line), Smagorinsky model (dashed line), standard SPH (+) and mSPH (\circ). Reproduced from Adami, X. Y. Hu, and N. A. Adams 2012

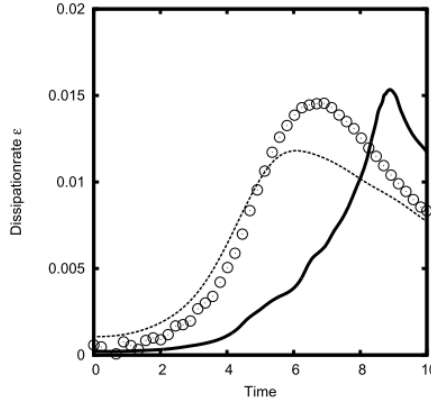


Figure 2.6: Dissipation rate at $Re = 3000$ using DNS (solid line), Smagorinsky model (dashed line) and mSPH (\circ). Reproduced from Adami, X. Y. Hu, and N. A. Adams 2012

2.2 Large Eddy Simulation-based Models

2.2.1 Implicit Pressure Poisson-based Models

Gotoh et al. (Hitoshi Gotoh, Songdong Shao, and Memita 2004) were amongst the first to integrate Large Eddy Simulation techniques with the SPH method. They derived this LES-SPH model, based on incompressible flow, to tackle the problem of reflection and transmission characteristics of regular waves by a partially immersed curtain-type breakwater. In order to compare the dissipation efficiencies, they considered the non-overtopping and overtopping cases of the problem.

The governing equations of the system were described as given by the continuity equation in Eq. 2.19 and the momentum equation in Eq. 2.17.

$$\frac{1}{\rho} \frac{D\rho}{Dt} + \nabla \cdot \mathbf{v} = 0 \quad (2.19)$$

The LES mass and momentum conservation equations for the flow were derived by filtering the respective equations using a spatial filter $\overline{(...)}$ to obtain their filtered counterparts as given by Eq. 2.20 and Eq. 2.21 respectively.

$$\frac{1}{\rho} \frac{D\rho}{Dt} + \nabla \cdot \bar{\mathbf{v}} = 0 \quad (2.20)$$

$$\frac{D\bar{\mathbf{v}}}{Dt} = -\frac{1}{\rho} \nabla \bar{P} + \nu \Delta(\bar{\mathbf{v}}) + \frac{1}{\rho} \nabla \cdot \underline{\tau} + \mathbf{F} \quad (2.21)$$

$$\frac{1}{\rho} \underline{\tau} = \bar{\mathbf{v}} \otimes \bar{\mathbf{v}} - \overline{\mathbf{v} \otimes \mathbf{v}} \quad (2.22)$$

The stress tensor ($\underline{\tau}$) defined in Eq. 2.22 is closed using Boussinesq's Hypothesis as defined in Eq. 2.23.

$$\frac{1}{\rho} \underline{\tau} = 2\nu_t \underline{S} - \frac{2}{3} k \underline{I} \quad (2.23)$$

The turbulent eddy viscosity is estimated using a modified Smagorinsky model as given in Eq. 2.24. This allows wall effects to be incorporated into the model,

which the authors required to tackle the problem they were working on.

$$\nu_t = \min(C_s \Delta x, \kappa d_{wall})^2 \sqrt{2 \langle \underline{S}, \underline{S} \rangle} \quad (2.24)$$

$$C_s = 0.1 \quad , \quad \kappa = 0.4 \quad (2.25)$$

Where (C_s) is the Smagorinsky constant, (κ) is the von Karman constant, d_{wall} is the normal distance of the particle to the closest wall, and (Δx) is the inter-particle spacing.

The first term in Eq. 2.24 dominates the flow far away from the solid wall, thereby recovering the standard Smagorinsky model. However, the second term dominates for flow close to the wall; hence, the eddy viscosity is a function of the particle distance to the wall. This overcomes the disadvantage of the standard Smagorinsky being over-dissipative inside the laminar layer.

In order to solve the system of equations and evolve them in time, the authors employed the Predictive-Corrective time integrator, similar to the two-step projection method of Chorin (Chorin 1968). The prediction stage is outlined by Eq. 2.26 - Eq. 2.28, where (δt) denotes the time step.

$$\Delta \mathbf{v}_* = \left(\nu \Delta(\bar{\mathbf{v}}) + \frac{1}{\rho} \nabla \cdot \underline{\tau} + \mathbf{F} \right) \Delta t \quad (2.26)$$

$$\mathbf{v}_* = \mathbf{v}_t + \Delta \mathbf{v}_* \quad (2.27)$$

$$\mathbf{r}_* = \mathbf{r}_t + \mathbf{v}_* \Delta t \quad (2.28)$$

The correction stage is outlined by Eq. 2.29 - Eq. 2.32. (\bar{P}) which is required to update the (\mathbf{v}_{t+1}) term is calculated implicitly from Eq. 2.30, which is based on the filtered continuity equation given by Eq. 2.20 and assuming incompressibility $\frac{D\rho}{Dt} = 0$.

$$\Delta \mathbf{v}_{**} = -\frac{1}{\rho} \nabla \bar{P}_{t+1} \Delta t \quad (2.29)$$

$$\nabla \cdot \left(\frac{1}{\rho_*} \nabla \bar{P}_{t+1} \right) = \frac{\rho_o - \rho_*}{\rho_o \Delta t^2} \quad (2.30)$$

$$\mathbf{v}_{t+1} = \mathbf{v}_* + \Delta \mathbf{v}_{**} \quad (2.31)$$

$$\mathbf{r}_{t+1} = \mathbf{r}_t + (\mathbf{v}_t + \mathbf{v}_{t+1}) \frac{\Delta t}{2} \quad (2.32)$$

In order to solve the system of equations given by Eq. 2.26 - Eq. 2.32 in an SPH setting, the authors presented the following SPH formulation for the flow property. The fluid density is given using a simple summation density Eq. 2.33.

$$\rho_i = \sum_j m_j W_{h,ij} \quad (2.33)$$

The pressure gradient term is defined in Eq. 2.34 in a symmetric form.

$$\left(\frac{1}{\rho} \nabla \bar{P} \right)_i = \sum_j m_j \left(\frac{\bar{P}_i}{\rho_i^2} + \frac{\bar{P}_j}{\rho_j^2} \right) \nabla_i W_{h,ij} \quad (2.34)$$

The divergence of \mathbf{v} is also defined symmetrically as given by Eq. 2.35.

$$\nabla \cdot \bar{\mathbf{v}}_i = \rho_i \sum_j m_j \left(\frac{\bar{\mathbf{v}}_i}{\rho_i^2} + \frac{\bar{\mathbf{v}}_j}{\rho_j^2} \right) \cdot \nabla_i W_{h,ij} \quad (2.35)$$

The pressure Laplacian, defined in Eq. 2.36, is formulated as a hybrid of a standard SPH first derivative with a finite difference approximation for the first derivative to aid particle pressure stability (Cummins and Rudman 1999).

$$\nabla \cdot \left(\frac{1}{\rho} \nabla \bar{P} \right)_i = \sum_j m_j \frac{8}{(\rho_i + \rho_j)^2} \frac{\bar{P}_{ij} \mathbf{r}_{ij} \cdot \nabla_i W_{h,ij}}{|\mathbf{r}_{ij}|^2} \quad (2.36)$$

The divergence of the stress tensor is defined in Eq. 2.37.

$$\left(\frac{1}{\rho} \nabla \cdot \underline{\boldsymbol{\tau}} \right)_i = \sum_j m_j \left(\frac{1}{\rho_i^2} \underline{\boldsymbol{\tau}}_i + \frac{1}{\rho_j^2} \underline{\boldsymbol{\tau}}_j \right) \cdot \nabla_i W_{h,ij} \quad (2.37)$$

Finally, the laminar stress term, consisting of the velocity Laplacian term, is defined as given by Eq. 2.38.

$$(\nu \Delta(\bar{\mathbf{v}}))_i = \sum_j m_j \frac{4(\eta_i + \eta_j)}{(\rho_i + \rho_j)^2} \frac{\bar{\mathbf{v}}_{ij} \mathbf{r}_{ij} \cdot \nabla_i W_{h,ij}}{|\mathbf{r}_{ij}|^2} \quad (2.38)$$

The authors used this SPH-LES model to investigate the wave interaction with a partially immersed breakwater and compared the results with experimentally obtained values of a similar setup. Their computational domain was 2D populated by $\approx 1.2 \times 10^4$ particles.

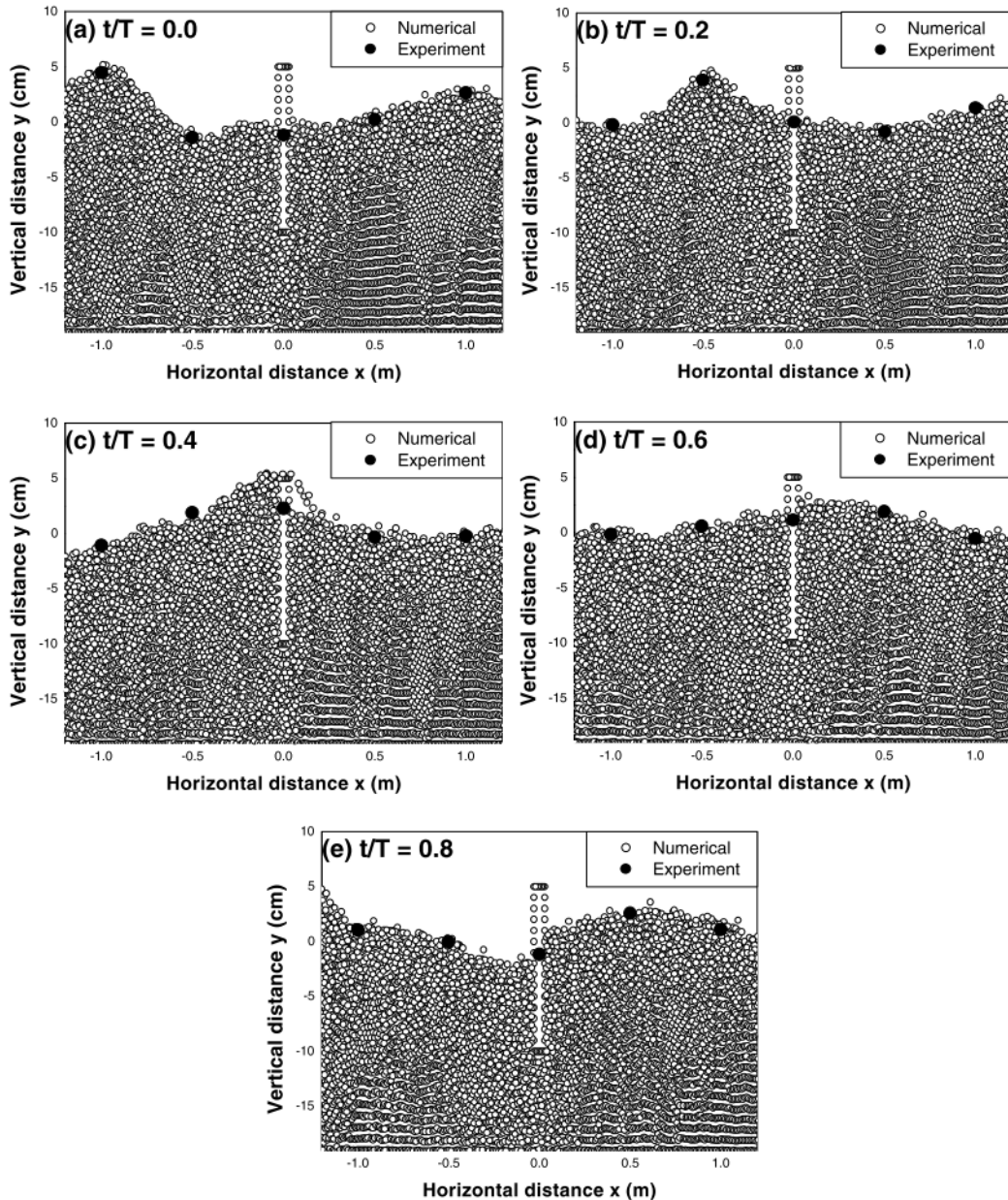


Figure 2.7: Time sequences of computational and experimental wave profiles near curtain wall (overtopping). Reproduced from Hitoshi Gotoh, Songdong Shao, and Memita 2004

As observed in the comparative plots given in Fig. 2.7, the model proves to be accurate in tracking free surfaces of large deformation without numerical diffusion. The authors also observed the model's capability to simulate turbulence and eddy vortices realistically near the curtain wall. However, the authors also conclude that a more refined turbulence model will be required for further accuracy in predicting flow involving wave interactions.

Building on the work mentioned above, Shao and Gotoh (Songdong Shao and Hitoshi Gotoh 2005) performed a comparative study of SPH and the Moving Particle Semi-Implicit (MPS) method coupled with an LES model. They also validated these models against experimental data.

The filtered conservation equations which the authors considered were the same

as given by Eq. 2.20 - Eq. 2.23. However, they incorporated the standard Smagorinsky model (Smagorinsky 1963) given by Eq. 2.39 as opposed to the modified model Eq. 2.24.

$$\nu_t = (C_s \Delta x)^2 \quad (2.39)$$

The authors consider the same predictive-corrective scheme to evolve their system as detailed in Eq. 2.26 - Eq. 2.32. Similarly, they follow the same SPH formulation outlined in Eq. 2.33 - Eq. 2.38. They do however, slightly modify the pressure and velocity Laplacian terms as given in Eq. 2.40 and Eq. 2.41 respectively.

$$(\nabla^2 P)_i = \sum_j m_j \frac{4}{\rho_i + \rho_j} \frac{P_{ij} \mathbf{r}_{ij} \cdot \nabla_i W_{h,ij}}{|\mathbf{r}_{ij}|^2} \quad (2.40)$$

$$(\nu \Delta(\mathbf{v}))_i = \sum_j m_j \frac{2(\nu_i + \nu_j)}{\rho_i + \rho_j} \frac{\mathbf{v}_{ij} \mathbf{r}_{ij} \cdot \nabla_i W_{h,ij}}{|\mathbf{r}_{ij}|^2} \quad (2.41)$$

The authors validated this SPH-LES Model using experimental data from the experimental data corresponding to a solitary wave breaking on the beach (Synolakis 1986). Their computational domain was 2D and consisted of $\approx 1.8 \times 10^4$ particles. From the computed wave profiles shown in Fig. 2.8, it can be visually observed that there is reasonable agreement between the experimental and computation data. This verifies the model's accuracy in tracking free surfaces with less or no numerical diffusion. Furthermore, by performing a convergence study of the SPH-LES model using the dam-break problem, the authors could show that the scheme's spatial and temporal accuracy is $O(\Delta t + \Delta x^{1.25})$.

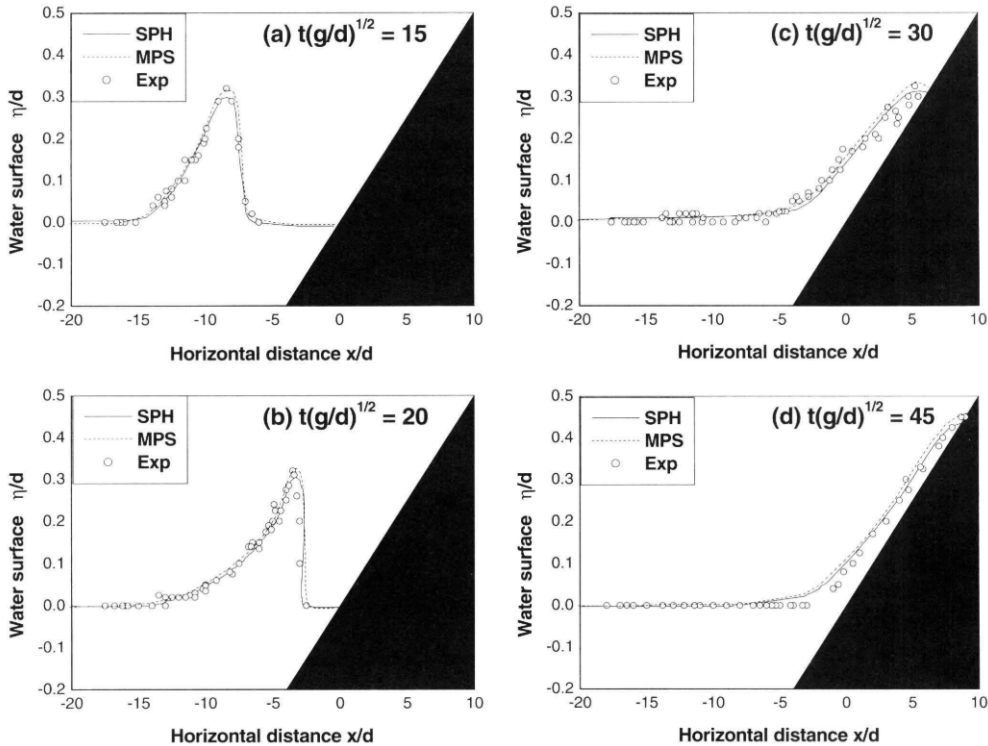


Figure 2.8: Experimental and computational wave profiles by SPH and MPS model. Reproduced from Songdong Shao and Hitoshi Gotoh 2005

2.2.2 Explicit Pressure Equation of State-based Models

Standard Smagorinsky Model

Rogers and Dalrymple (ROGERS and DALRYMPLE 2005), similar to the work on SPH-LES modelling detailed in Sec. 2.2.1, came up with an LES-type sub-particle-scale (SPS) formulation based on the weakly compressible assumption in order to develop a turbulence model for SPH.

The authors considered the mass and momentum conservation equations as already given in Eq. 2.19 and Eq. 2.17 respectively, along with the equation of state Eq. 2.1. However, for the value of (B) in the state equation, the authors considered the definition given in Eq. 2.42:

$$B' = 10u_{max} \quad (2.42)$$

Where (u_{max}) is the maximum particle velocity.

They subsequently filtered the compressible conservation equations using Favre averaging as given by Eq. 2.43.

$$\tilde{f} = \frac{\overline{\rho f}}{\overline{\rho}} \quad (2.43)$$

The derived filtered conservation equations for mass and momentum are detailed in Eq. 2.44 and Eq. 2.45.

$$\frac{D\bar{\rho}}{Dt} = -\bar{\rho}\nabla \cdot \tilde{\mathbf{v}} \quad (2.44)$$

$$\frac{D\tilde{\mathbf{v}}}{Dt} = -\frac{1}{\bar{\rho}}\nabla\bar{P} + \frac{1}{\bar{\rho}}(\nabla \cdot \bar{\rho}\nu\nabla)\tilde{\mathbf{v}} + \frac{1}{\bar{\rho}}\nabla \cdot \underline{\tau} + \mathbf{F} \quad (2.45)$$

Where the SPS stress tensor and turbulent eddy viscosity is given by Eq. 2.46 and Eq. 2.47 respectively.

$$\underline{\tau} = \bar{\rho}\left(2\nu_t\underline{S} - \frac{2}{3}\text{tr}[\underline{S}]\underline{I}\right) - \frac{2}{3}\bar{\rho}C_I\bar{\Delta}^2\underline{I} \quad , \quad C_I = 6.6 \times 10^{-4} \quad (2.46)$$

$$\nu_t = (C_s\Delta x)^2\sqrt{2\langle \underline{S}, \underline{S} \rangle} \quad , \quad C_s = 0.12 \quad (2.47)$$

As for the SPH formulations of the aforementioned governing equations, the authors

The authors derived the SPH formulations of the aforementioned governing equations. The continuity equation takes the form as detailed in Eq. 2.2. The pressure gradient term is given in Eq. 2.34. The laminar stress term, consisting of the velocity Laplacian is given by Eq. 2.48, which itself was built on the work of Morris et al. (Morris, Fox, and Zhu 1997) as given in Eq. 2.49. Finally the stress divergence is defined by Eq. 2.37.

$$\left(\frac{1}{\rho}(\nabla \cdot \eta\nabla)\mathbf{v}\right)_i = \sum_j m_j \frac{\nu(\rho_i + \rho_j)}{\rho_{ij}^2} \frac{\mathbf{v}_{ij}\mathbf{r}_{ij} \cdot \nabla_i W_{h,ij}}{|\mathbf{r}_{ij}|^2 + \zeta^2} \quad (2.48)$$

$$\left(\frac{1}{\rho}(\nabla \cdot \eta\nabla)\mathbf{v}\right)_i = \sum_j m_j \frac{(\eta_i + \eta_j)\mathbf{v}_{ij}}{\rho_i\rho_j} \left(\frac{1}{|\mathbf{r}_{ij}|} \frac{\partial W_{h,ij}}{\partial r_i}\right) \quad , \quad \nabla_i W_{h,ij} = \frac{\mathbf{r}_{ij}}{|\mathbf{r}_{ij}|} \frac{\partial W_{h,ij}}{\partial r_i} \quad (2.49)$$

The authors noted that the LES description of viscous effects in slightly compressible SPH could lead to unphysical behaviour at free surfaces due to density

variations being magnified by the equation of state. The lack of artificial viscosity implies that such variations are not damped. They subsequently noted that averaging the density would ensure smooth and physically acceptable free surfaces, based on the work of Panizzo (Panizzo 2004). Hence, they performed Shepard filtering of the density as defined in Eq. 2.50 every 40-time steps.

$$\rho_i = \frac{\sum_j \rho_j W_{h,ij} \mathcal{V}_j}{\sum_j W_{h,ij} \mathcal{V}_j} \quad (2.50)$$

The authors simulated the problem of a weakly plunging breaker in 2D and 3D to ascertain the performance and capability of the model. Their 2D computational domain consisted of $\approx 1 \times 10^5$ particles, with the 3D domain consisting $\approx 2 \times 10^4$ particles. The authors could show that in the case of the 2D problem, the model could predict regions of high vorticity that persisted longer when compared to standard SPH utilising conventional artificial viscosity. The model also displayed the turbulent bore, which generated reverse breaking, leading to the downbursting-like phenomenon, as observed in experiments (Kubo and Sunamura 2001). In the case of the 3D problem, the authors showed the model's capability to capture near vertically-oriented eddies despite the lower resolution.

Building on this work, Dalrymple and Rogers (Dalrymple and Rogers 2006) used this scheme on a wide variety of problems, ranging from 2D Green water overtopping, 2D waves on a beach, 3D dam break and 3D waves on a beach. The quantitative analysis of the results allowed the authors to conclude that the model is especially suited for problems involving splash or flow separation. The authors also warn about the model's requirement of a large number of particles for sufficient resolution. That and the finite speed of sound stemming from the compressible flow implied that time steps had to $O(10^{-5}s)$. Hence, the authors remain cautiously optimistic about the model since the method performs well for smaller regions where the number of particles is reasonable. However, they believe that extended Boussinesq codes would more efficiently model larger domains.

Modified Smagorinsky Model

Canelas et al. (Canelas et al. 2016) constructed the wall-adapting local eddy viscosity (WALE) model to be incorporated in the SPH-LES scheme. They noted that studying turbulent flow fields required the identification of vortices themselves to study their interactions in the flow. They used the definition of Lagrangian Coherent Structures (LCS) to help capture these vortices. As a Lagrangian method, SPH is preferable for studying LCS since the technique provides the motion of individual fluid particles, thereby eliminating the need for expensive post-processing inherent to Eulerian solutions. However, they noted that typically employed SPS strategies for LES simulations, based on the standard Smagorinsky model, cannot correctly enforce wall conditions and non-vanishing stresses with laminar flows. Hence they devised the WALE model.

The authors consider the compressible Navier-Stokes (NS) along the continuity equation as their governing equation. They subsequently present the SPH formulation of the continuity equation as defined by Eq. 2.51.

$$\frac{D \rho_i}{D t} = -\rho_i \sum_j m_j \mathbf{v}_{ij} \cdot \nabla_i W_{h,ij} \quad (2.51)$$

The pressure gradient term is given in Eq. 2.34. The laminar stress term, consisting of the velocity Laplacian, is given by Eq. 2.52.

$$(\nu \Delta(\mathbf{v}))_i = \sum_j m_j \frac{4\nu}{\rho_i + \rho_j} \frac{\mathbf{v}_{ij} \mathbf{r}_{ij} \cdot \nabla_i W_{h,ij}}{|\mathbf{r}_{ij}|^2} \quad (2.52)$$

Finally the stress divergence is defined by Eq. 2.37, with the stress tensor being defined by Eq. 2.53

$$\underline{\tau} = \rho \left(2\nu_t \underline{S} - \frac{2\nu_t}{3} \text{tr}[\underline{S}] \underline{I} \right) - \left(\frac{4}{3} \rho C_I (\Delta x)^2 \langle \underline{S}, \underline{S} \rangle \right) \underline{I} \quad , \quad C_I = 6.6 \times 10^{-3} \quad (2.53)$$

The WALE model redefines the turbulent eddy viscosity as given by Eq. 2.54.

$$\nu_t = \rho (C_w \Delta x)^2 \frac{\langle \underline{S}^d, \underline{S}^d \rangle^{3/2}}{\langle \underline{S}, \underline{S} \rangle^{5/2} + \langle \underline{S}^d, \underline{S}^d \rangle^{5/4}} \quad , \quad C_w = 0.325 \quad (2.54)$$

$$\underline{S}^d = \frac{1}{2} \left((\nabla \mathbf{v})^2 + ((\nabla \mathbf{v})^T)^2 \right) - \frac{1}{3} \text{tr}[(\nabla \mathbf{v})^2] \underline{I} \quad (2.55)$$

In order to test their model, the authors considered an array of cylinders in fluid flow as shown in Fig. 2.9, with a constant body force. They computed the vorticity field and the Finite-Time Lyapunov Exponents (FTLE) field to study the LCSs in the flow. These fields are shown in Fig. 2.10 and Fig. 2.11 respectively.

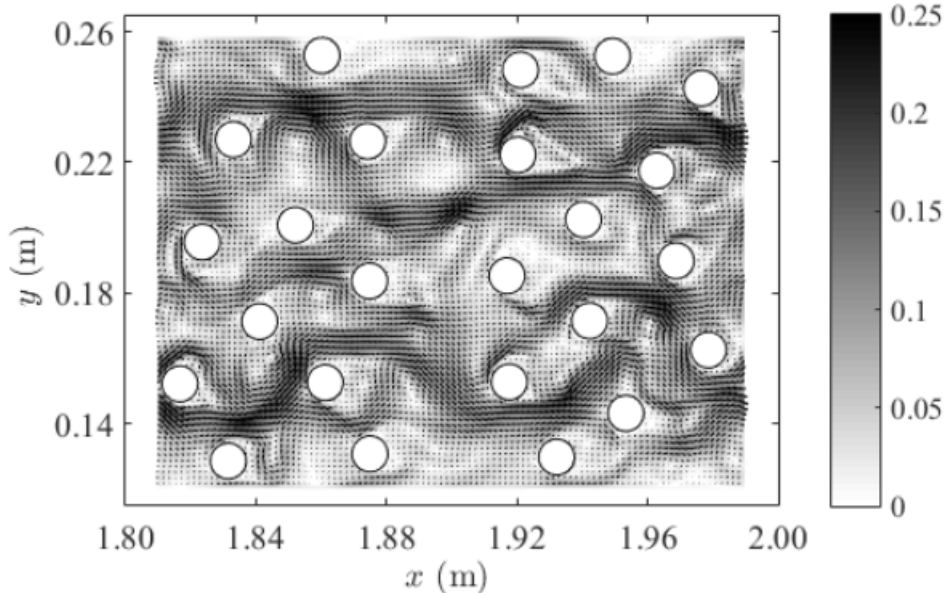


Figure 2.9: Cylinder distribution and instantaneous velocity overlapped by velocity vectors. Velocity in m/s , at $t = 20s$. The flow direction is from left to right. Reproduced from Canelas et al. 2016

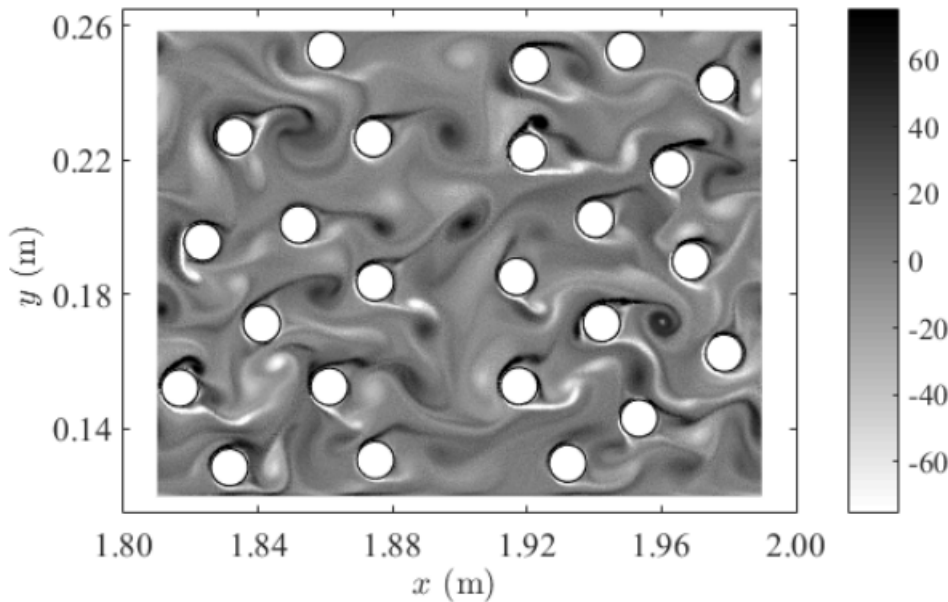


Figure 2.10: Vorticity field. Vorticity in Hz, at $t = 20\text{s}$. Reproduced from Canelas et al. 2016

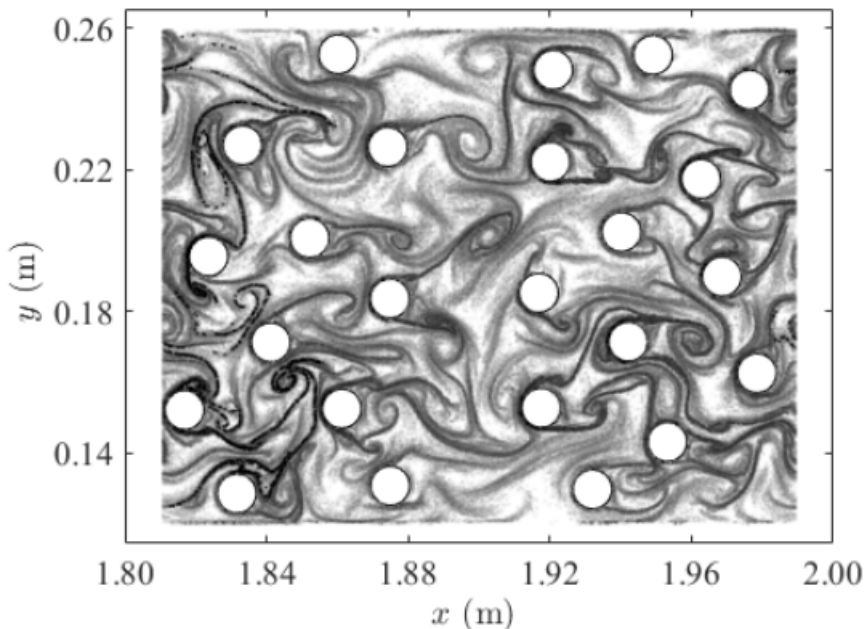


Figure 2.11: FTLE field with negative integration time ($T = -0.4\text{s}$) (unstable manifolds - attracting LCS) at $t = 20\text{s}$. Reproduced from Canelas et al. 2016

Okraschevski et al. (Okraschevski et al. 2022), building on the work of Hardy (Hardy 1982), show that SPH should be viewed as a Lagrangian quadrature technique for the governing equations of explicit LES, raising interesting implications for SPH as a method itself. Firstly, the kernel scale limits SPH's physical resolution, rendering it unsuitable as a DNS alternative. Secondly, any deficits introduced below the kernel scale could be resolved by consideration of the stress term, from

which structures above the kernel scale could benefit. The authors consider this second implication a working hypothesis to try and prove or disprove.

The authors use the compressible NS equations and subject them to a spatial average to obtain the filtered governing equations. They subsequently derive the SPH formulations of the mass and momentum conservation equations as given in Eq. 2.15 and Eq. 2.56.

$$\bar{\rho}_i \frac{D \tilde{\mathbf{v}}}{Dt} = - \sum_j (\bar{P}_i + \bar{P}_j) \nabla_i W_{h,ij} \mathcal{V}_j + 2(2 + n_{dim}) \eta \sum_j \frac{\tilde{\mathbf{v}}_{ij} \cdot \mathbf{r}_{ij}}{|\mathbf{r}_{ij}|^2} \nabla_i W_{h,ij} \mathcal{V}_j + \nabla \cdot \underline{\tau} \quad (2.56)$$

Where (n_{dim}) denotes the number of spatial dimensions for a given problem.

The equation of state is given by Eq. 2.57, with the SFS tensor being given by Eq. 2.58.

$$\bar{P}_i = P_o + K \left(\frac{\bar{\rho}_i}{\rho_o} - 1 \right) \quad (2.57)$$

Where, (K) is a constant.

$$\underline{\tau} = 2\nu_t \bar{\rho} \underline{S} \quad (2.58)$$

The SPH formulation for the strain rate tensor is given by Eq. 2.59, and the divergence of the SFS tensor being given by Eq. 2.60.

$$\underline{S}_i = - \sum_j \tilde{\mathbf{v}}_{ij} \otimes \nabla_i W_{h,ij} \mathcal{V}_j \quad (2.59)$$

$$\left(\nabla \cdot \underline{\tau} \right)_i = \sum_j (\underline{\tau}_i + \underline{\tau}_j) \nabla_i W_{h,ij} \mathcal{V}_j \quad (2.60)$$

The authors consider three models for the turbulent eddy viscosity:

- SMAG: Standard Smagorinsky model

$$\nu_t = (C_s \Delta x)^2 \sqrt{2 \langle \underline{S}, \underline{S} \rangle} \quad (2.61)$$

- SIGMA: σ -model (Nicoud et al. 2011), where (σ_i) denotes the i^{th} singular value of the velocity gradient

$$\nu_t = (C_\sigma \Delta x)^2 \frac{\sigma_3(\sigma_1 - \sigma_2)(\sigma_2 - \sigma_3)}{\sigma_1^2} \quad (2.62)$$

- SMAG-MCG: Standard Smagorinsky model discretized in the Monaghan-Cleary-Gingold (MCG) form (Cleary and Joseph J Monaghan 1999)

$$\nabla \cdot \underline{\tau} = 2(2 + n_{dim}) \sum_j \bar{\rho}_i \bar{\rho}_j \frac{\nu_{t,i} + \nu_{t,j}}{\bar{\rho}_i + \bar{\rho}_j} \frac{\tilde{\mathbf{v}}_{ij} \cdot \mathbf{r}_{ij}}{|\mathbf{r}_{ij}|^2} \nabla_i W_{h,ij} \mathcal{V}_j \quad (2.63)$$

The authors show a correlation between the vorticity and SFS tensor. They subsequently conclude that the fluctuations in the vorticity, energy spectra and SFS tensor are correlated quantities that contain different information about the numerical dissipation dynamics.

The authors use the 3D TGV problem to study and investigate the proposed models. They consider various resolutions to study the problem, varying from $\approx 200^3 - 500^3$ particles.

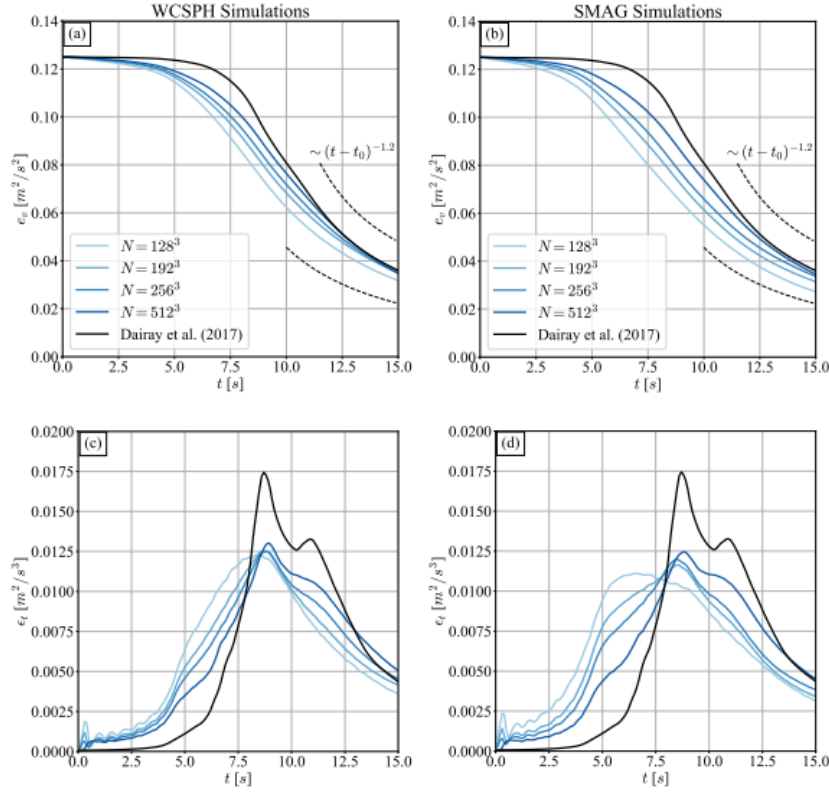


Figure 2.12: Comparison of quantitative metrics for different particle counts N . (a) & (b) Temporal evolution of the density-weighted averaged kinetic energy. (c) & (d) Temporal evolution of the averaged dissipation rate. Reproduced from Okrashevski et al. 2022

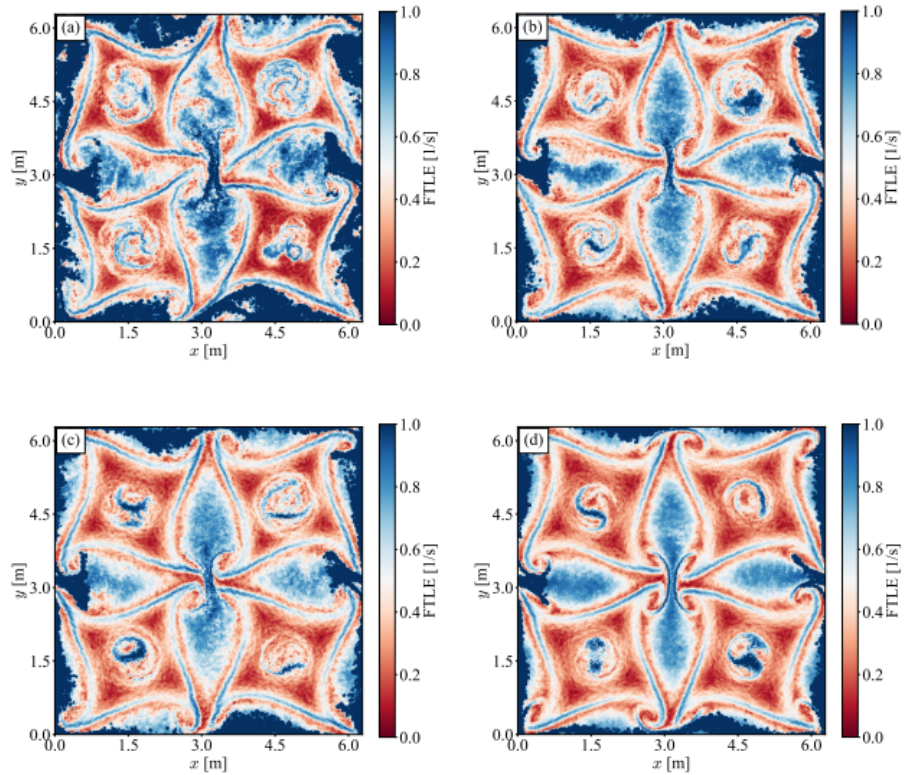


Figure 2.13: Backward FTLE at the plane $z = \pi$ for $N = 2563$ and $t = 14\text{s}$ in the range $[11; 14]\text{s}$. (a) Without explicit SFS model. (b) With the SMAg model. (c) With SIGMA model. (d) With the SMAg-MCG model. Reproduced from Okrashevski et al. 2022

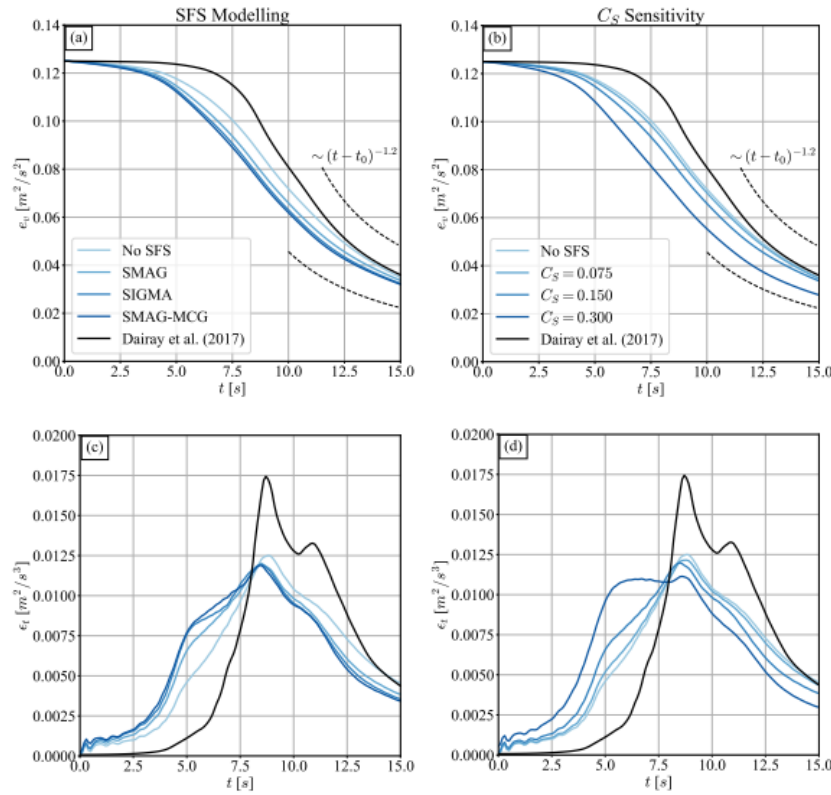


Figure 2.14: Comparison of quantitative metrics for different $N = 256^3$ runs. (a) & (b) Temporal evolution of the density-weighted averaged kinetic energy. (c) & (d) Temporal evolution of the averaged dissipation rate. Reproduced from Okrashevski et al. 2022

The SMAG model degrades the flow in terms of the averaged kinetic energy in Fig. 2.12 (b) and the corresponding dissipation rate in Fig. 2.12 (d). This negative attribute of the model outweighs the positive attribute of the model, in that cases with the SMAG model in Fig. 2.13 (b) appear less tattered and exhibit symmetry compared to the reference WCSSPH solution in Fig. 2.13 (a). From Fig. 2.14, it becomes evident that with larger (C_s), the averaged kinetic energy is increasingly reduced, which is also reflected by the dissipation rates. This indicates that the best choice corresponds to ($C_s \rightarrow 0$).

On a concluding note, the authors claim that the subsonic turbulence captured by SPH can correctly represent the flow field up to the kernel scale but at a high cost in the best of cases. They also note that explicit SFS models, at most, only lead to marginal improvement of LCS. However, regarding the inertial range dynamics, the dissipative SFS models remove kinetic energy, which is highly detrimental since a spectral energy deficit already characterises SPH. The authors attribute these drawbacks to the non-local character of the Lagrangian quadrature, which they explain through the concept of *Particle Duality*. The concept states that the SPH particles must represent superfluid element approximants and fluid element surrogates simultaneously, leading to an unphysical increase in particle interaction distances. The authors, hence prove Rennehan's expectation that explicit SFS models in an SPH framework can only degrade the quality of the approximation for subsonic turbulent flow (Rennehan 2021), which raises concerns for turbulence modelling in SPH. However, the authors note there might be hope from SPH native models.

2.3 Lagrangian LES-based Models

Having reviewed turbulence models developed for SPH, Di Mascio et al. (Di Mascio et al. 2017) concluded that LES models could serve as an excellent middle ground between RANS and DNS. This is because only the sub-grid scale eddies would be modelled, allowing for the larger eddies to be directly simulated from the NS equations. They also note that contemporary SPH-LES models use the Eulerian differential operators in an SPH formulation and therefore do not have a rigorous background. Therefore they propose a Lagrangian form of LES to tie in with the Lagrangian quadrature technique, that is, SPH.

The authors consider a weakly compressible, barotropic fluid whose conservation equations for mass and density are given by Eq. 2.19 and Eq. 2.64 respectively.

$$\frac{D\mathbf{v}}{Dt} = -\frac{1}{\rho} + \nu\Delta(\mathbf{v}) + (\lambda' + \nu)\nabla(\nabla \cdot \mathbf{v}) \quad (2.64)$$

Where, $(\lambda' = \lambda/\rho)$ is the Lamé constant. The equation of state is simply given as Eq. 2.65.

$$P = F(\rho) \quad (2.65)$$

$$\frac{D\mathbf{r}}{Dt} = \mathbf{v} \quad (2.66)$$

The authors subsequently define a Lagrangian filter (ϕ) with compact support of the form

$$\phi = \phi(\tilde{\mathbf{r}}_p(t) - \mathbf{y}, t - \tau) \quad (2.67)$$

Where the filter is an even function in its arguments, and $(\tilde{\mathbf{r}}_p(t))$ is the position of a material which moves with velocity

$$\tilde{\mathbf{v}}(\tilde{\mathbf{r}}, t) = \int_{\mathbb{R}^3} \int_{-\infty}^{\infty} \phi(\tilde{\mathbf{r}}_p(t) - \mathbf{y}, t - \tau) \mathbf{v}(\mathbf{y}, \tau) d\tau dV_y \quad (2.68)$$

By using the filter as defined in Eq. 2.67, the filtered governing equations are as follows

$$\frac{D\tilde{\rho}}{Dt} = -\tilde{\rho}\nabla \cdot \tilde{\mathbf{v}} + \nabla \cdot (\tilde{\rho}\tilde{\mathbf{v}} - \tilde{\rho}\mathbf{v}) \quad (2.69)$$

$$\frac{D\tilde{\mathbf{v}}}{Dt} = -\frac{\nabla \tilde{P}}{\tilde{\rho}} + \nu\Delta(\tilde{\mathbf{v}}) + (\lambda' + \nu)\nabla(\nabla \cdot \tilde{\mathbf{v}}) - \nabla[(\tilde{\rho}) - G(\tilde{\rho})] + \nabla \cdot \underline{\mathbf{T}}_l + \widetilde{\mathbf{v}\nabla \cdot \mathbf{v}} \quad (2.70)$$

$$\frac{D\tilde{\mathbf{r}}}{Dt} = \tilde{\mathbf{v}} \quad (2.71)$$

$$\tilde{\rho} = F(\tilde{P}) \quad (2.72)$$

$$\underline{\mathbf{T}}_l = \tilde{\mathbf{v}} \otimes \tilde{\mathbf{v}} - \widetilde{\mathbf{v} \otimes \mathbf{v}} \quad (2.73)$$

$$G(\rho) = \int^{\rho} \frac{1}{s} \frac{dF}{ds} ds \quad (2.74)$$

In order for the authors to be able to reinterpret the Lagrangian LES through SPH, they split the filter as follows

$$\phi(\tilde{\mathbf{r}}_p(t) - \mathbf{y}, t - \tau) = W(\tilde{\mathbf{r}} - \mathbf{y})\theta(t - \tau) \quad (2.75)$$

This allows the author to provide a relationship between the various type of filtered quantities as given

$$\langle f \rangle(\tilde{\mathbf{r}}, t) = \int_{\mathbb{R}^3} W(\tilde{\mathbf{r}} - \mathbf{y}) f(\mathbf{y}, t) dV_y \quad (2.76)$$

$$\bar{f}(\mathbf{y}, t) = \int_{\mathbb{R}} \theta(t - \tau) f(\mathbf{y}, \tau) d\tau \quad (2.77)$$

$$\tilde{f} = \langle \bar{f} \rangle, \langle \bar{f} \rangle \neq \langle \tilde{f} \rangle \quad (2.78)$$

The authors, therefore, can derive the equations in an SPH formalism as given by

$$\frac{D\tilde{\rho}}{Dt} = -\tilde{\rho}\langle \nabla \cdot \tilde{\mathbf{v}} \rangle + C_1 + C_2 \quad (2.79)$$

$$C_1 = -\tilde{\rho}\langle \nabla \cdot (\tilde{\mathbf{v}} - \bar{\mathbf{v}}) \rangle \quad (2.80)$$

$$C_2 = \nabla \cdot (\tilde{\rho}\tilde{\mathbf{v}} - \bar{\rho}\bar{\mathbf{v}}) \quad (2.81)$$

$$\frac{D\tilde{\mathbf{v}}}{Dt} = -\frac{\langle \nabla \tilde{P} \rangle}{\tilde{\rho}} + \nu \langle \Delta(\tilde{\mathbf{v}}) \rangle + (\lambda' + \nu) \langle \nabla(\nabla \cdot \tilde{\mathbf{v}}) \rangle + M_1 + M_2 \quad (2.82)$$

$$M_1 = -\frac{\langle \nabla(\bar{\rho} - \tilde{\rho}) \rangle}{\tilde{\rho}} + \nu \langle \Delta(\bar{\mathbf{v}} - \tilde{\mathbf{v}}) \rangle + (\lambda' + \nu) \langle \nabla(\nabla \cdot (\bar{\mathbf{v}} - \tilde{\mathbf{v}})) \rangle \quad (2.83)$$

$$M_2 = -\nabla(\widetilde{G(\rho)} - G(\tilde{\rho})) + \widetilde{\mathbf{v}\nabla \cdot \mathbf{v}} + \nabla \cdot \underline{\mathbf{T}}_l \quad (2.84)$$

$$\frac{D\tilde{\mathbf{r}}}{Dt} = \tilde{\mathbf{v}} \quad (2.85)$$

$$\tilde{P} = F(\tilde{\rho}) \quad (2.86)$$

The authors close the terms (C_2, M_2) as follows

$$C_2 \approx \nabla \cdot (\nu_\delta \nabla \tilde{\rho}), \quad (2.87)$$

$$\nu_\delta = (C_\delta \sigma)^2 \sqrt{2 \langle \underline{\mathbf{S}}, \underline{\mathbf{S}} \rangle} \quad (2.88)$$

Where (ν_δ) has the dimensions of kinematic viscosity and represents a turbulent diffusion coefficient, (C_δ) represents a dimensionless coefficient, and ($\sigma \propto h$). If the spatial derivative of (ν_δ) is negligible then

$$C_2 = \nu_\delta \Delta(\tilde{\rho}) \quad (2.89)$$

$$M_2 = \nabla \cdot \underline{\mathbf{T}}_l = \nabla \cdot \left(-\frac{k^2}{3} \underline{\mathbf{I}} - \frac{2}{3} \nu_t \text{Tr}[\tilde{\underline{\mathbf{S}}} \underline{\mathbf{I}}] + 2\nu_t \tilde{\underline{\mathbf{S}}} \right) \quad (2.90)$$

$$k^2 = 4C_y \sigma^2 \langle \underline{\mathbf{S}}, \underline{\mathbf{S}} \rangle, \quad C_y = 0.044 \quad (2.91)$$

$$\nu_t = (C_s \sigma)^2 \sqrt{2 \langle \underline{\mathbf{S}}, \underline{\mathbf{S}} \rangle}, \quad C_s = 0.12 \quad (2.92)$$

Where ($\text{Tr}[]$) is the trace operator, (C_y) is the Yoshizawa constant (Yoshizawa 1986), and (C_s is the Smagorinsky constant).

The above equations, coupled with the closure models, allow the authors to replace the differential operators with SPH counterparts of WCSPH.

The authors used the 2D and 3D TGV problems to validate the model. The authors considered Reynolds number up to $\approx 1.2 \times 10^5$ for the 2D case, and $\approx 1.5 \times 10^3$ for the 3D case. The authors also compared the proposed model against that of the

DNS SPH scheme, which was developed by Mayrhofer et al. (Mayrhofer et al. 2015) as observed in Fig. 2.15 and Fig. 2.16.

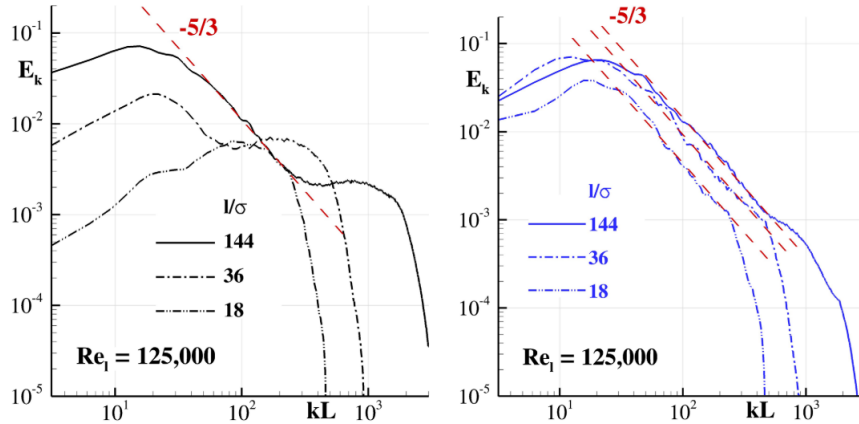


Figure 2.15: 2D freely decaying turbulence ($tU/L = 2, Re = 1.25 \times 10^5$). Left: Energy spectrum using DNS-SPH. Right: Energy spectrum using LES-SPH. Reproduced from Di Mascio et al. 2017

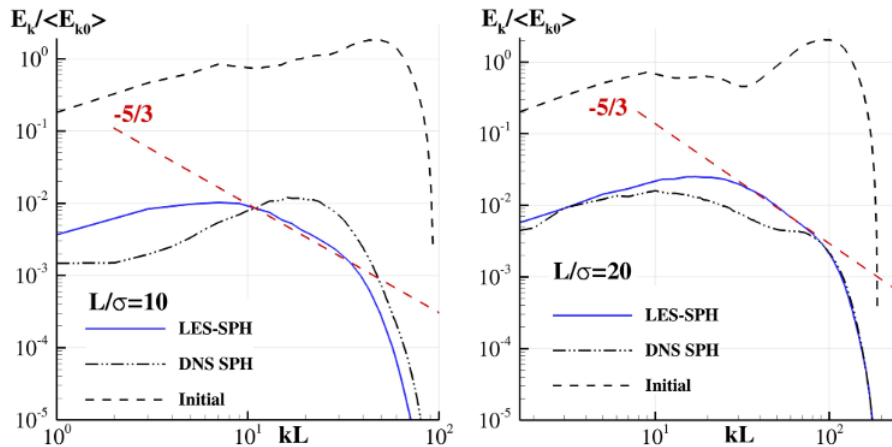


Figure 2.16: 3D homogeneous turbulence decay. Comparison between DNS-SPH and LES-SPH simulations ($tU/L = 5$). Left: Particle resolution = 64^3 . Right: particle resolution = 128^3 . Reproduced from Di Mascio et al. 2017

As seen from the results of the simulations in Fig. 2.15 and Fig. 2.16 for the 2D and 3D case, respectively, the authors were able to claim that the model captures the typical characteristics of the flow evolution with relatively coarse particle discretisation, provided an appropriate LES modelling is used.

Building on this, Colagrossi et al. (Colagrossi 2021) introduced a small arbitrary velocity deviation ($\delta\tilde{\mathbf{v}}$) to the fluid particle as given by

$$\frac{D\tilde{\mathbf{r}}}{Dt} = \tilde{\mathbf{v}} + \delta\tilde{\mathbf{v}} \quad (2.93)$$

This was done since the Lagrangian nature of the proposed model was proving to be an obstacle for accurate simulations of high Reynolds number problems. Therefore, they modified the model with the transport equation given in Eq. 2.93 to obtain

a quasi-Lagrangian LES-SPH model. The small velocity deviation to the actual Lagrangian velocity was based on the work done on particle shifting technique (PST) and tensile instability control (TIC) technique by Sun et al. (Sun, Andrea Colagrossi, et al. 2018) in their δ -SPH scheme.

The authors subsequently employed this δ -LES-SPH scheme with the same set of closure models as detailed by DiMascio et al. (Di Mascio et al. 2017). They compared their proposed model with standard LES-SPH on the 2D and 3D TGV problems for Reynolds numbers up to 1×10^6 .

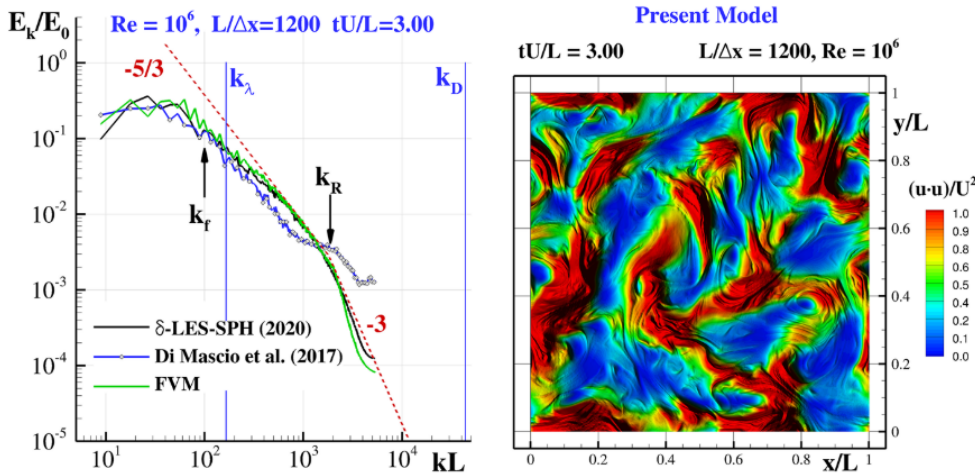


Figure 2.17: Left: Energy spectrum at ($tU/L = 3, Re = 1 \times 10^6$) as predicted by the δ -LES-SPH model and a finite volume scheme. Symbols k_f and k_R indicate the wave numbers of the external forcing and the kernel radius, respectively, while k_λ and k_D are the wave numbers associated with the Taylor and Kolmogorov scales. Right: k field at the same instant. Reproduced from Colagrossi 2021

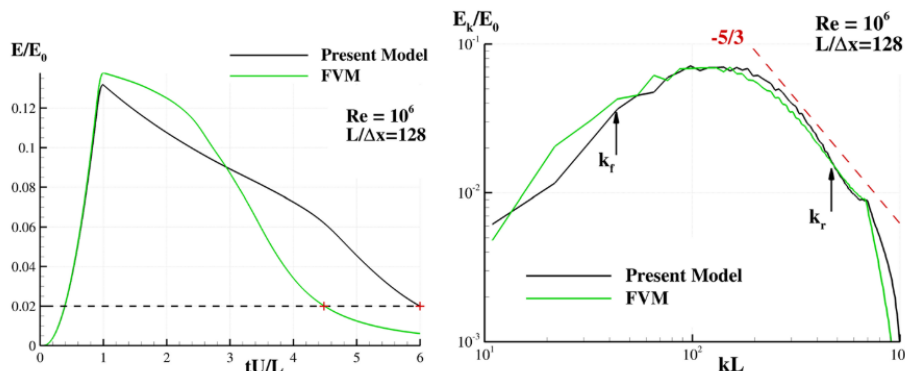


Figure 2.18: Left: Time histories of k as predicted by finite volume scheme and the δ -LES-SPH model. Right: Energy spectra. Symbols k_f and k_R denote the wave numbers of the external forcing and the kernel radius, respectively. Reproduced from Colagrossi 2021

As seen from the results of the simulations in Fig. 2.17 and Fig. 2.18 for the 2D and 3D case respectively, the authors claimed that the proposed model could overcome issues of high Reynolds number flows, such as generation of spurious high-frequency noise and the onset of the tensile instability. Furthermore, comparing the

proposed model's and an FVM solve's energy spectra with the theoretical decay rate confirmed the model's accuracy and reliability.

The authors conclude that the δ -LES-SPH model would need to be validated for flows with a Reynolds number larger than 1×10^6 with experimental or numerical data. They believe that the inclusion of wall functions to deal with solid boundaries and the extension of the model to free-surface flows can further improve the model's effectiveness. Finally, the authors believe that a higher-order approach could significantly improve the model results.

2.3.1 Extension to EDAC-SPH Scheme

The Entropically Damped Artificial Compressibility (EDAC) SPH scheme, based on the work of (Clausen 2013), is an explicit SPH method devised for incompressible flow by (Ramachandran and Puri 2019). In this scheme, the authors consider a transport equation for pressure instead of density derived from the continuity equation, as given in Eq. 2.94.

$$\frac{D P}{D t} = -c_s^2 \rho \nabla \cdot \mathbf{v} + \nu \nabla^2 P \quad (2.94)$$

Considering the pressure evolution equation above, an equation of state is longer required by the scheme. By filtering Eq. 2.94 with the Lagrangian LES technique (Di Mascio et al. 2017), we arrive at the result given by Eq. 2.95 (Refer Appendix A for derivation).

$$\frac{D \tilde{P}}{D t} = -c_s^2 \rho \nabla \cdot \tilde{\mathbf{v}} + \nu \nabla^2 \tilde{P} + \tilde{\mathbf{v}} \cdot \nabla \tilde{P} - \widetilde{\mathbf{v} \cdot \nabla P} \quad (2.95)$$

In Eq. 2.95, we see that the term $(\widetilde{\mathbf{v} \cdot \nabla P})$ cannot be reduced further to a form of $(f(\tilde{\mathbf{v}}, \tilde{P}))$. Hence, we cannot proceed with the SPH formulation for the pressure equation, implying that the EDAC scheme might not be compatible with the Lagrangian LES model.

2.4 RANS-based $k - \epsilon$ Models

Shao (Songdong Shao 2006) demonstrated that the two-equation $k - \epsilon$ model, an extensively studied model derived from the Reynolds-averaged Navier–Stokes (RANS) equations, can be incorporated in the truly incompressible version of SPH (ISPH). By attempting to extend RANS equations, which are hugely successful in practical fields, to a mesh-free method such as SPH, the author provides a framework to build on the wide variety of closure models available.

To discretise the RANS equations to an SPH form, the author considers the Reynolds averaged mass and momentum conservation equations as given in Eq. 2.96 and Eq. 2.97 respectively. Note: The averaged flow properties are represented without any over-line (...) hereafter.

$$\frac{1}{\rho} \frac{D \rho}{D t} + \nabla \cdot \mathbf{v} = 0 \quad , \quad \frac{D \rho}{D t} = 0 \text{ (Incompressible)} \quad (2.96)$$

$$\frac{D \mathbf{v}}{D t} = -\frac{1}{\rho} \nabla P + \nu \Delta(\mathbf{v}) + \frac{1}{\rho} \nabla \cdot \underline{\tau} + \mathbf{F} \quad (2.97)$$

The stress tensor is given by Eq. 2.23, while the turbulent eddy viscosity is defined as Eq. 2.98.

$$\nu_t = c_d \frac{k^2}{\epsilon} \quad (2.98)$$

The transport equations for the turbulent kinetic energy and dissipation rate is given by Eq. 2.99 and Eq. 2.100 respectively.

$$\frac{Dk}{Dt} = \nabla \cdot \left(\frac{\nu_t}{\sigma_k} \nabla k \right) + P_k - \epsilon \quad (2.99)$$

$$\frac{D\epsilon}{Dt} = \nabla \cdot \left(\frac{\nu_t}{\sigma_\epsilon} \nabla \epsilon \right) + c_{1\epsilon} \frac{\epsilon}{k} P_k - c_{2\epsilon} \frac{\epsilon^2}{k} \quad (2.100)$$

$$P_k = 2\nu_t \langle \underline{S}, \underline{S} \rangle \quad (2.101)$$

Where, $(\sigma_k, \sigma_\epsilon, c_{1\epsilon}, c_{2\epsilon}) = (1.0, 1.3, 1.44, 1.92)$ are empirical constants dependent on the nature of the flow , and (P_k) is the turbulence production rate, which satisfies the relation given by Eq. 2.102 (Stephen B Pope and Stephen B Pope 2000).

$$\frac{P_k}{\epsilon} = c_d \left(\frac{\sqrt{2\langle \underline{S}, \underline{S} \rangle}}{\epsilon} \right) \quad (2.102)$$

These governing equations are solved and evolved using the same predictive-corrective time integrator as seen in the work of (Hitoshi Gotoh, Songdong Shao, and Memita 2004), and outlined in Eq. 2.26 - Eq. 2.32.

As for the SPH formulations of the governing equations, the author builds on the work of (Hitoshi Gotoh, Songdong Shao, and Memita 2004), and uses the same discretization as defined in Eq. 2.33 - Eq. 2.37. However, the author uses a slightly modified version of the laminar stress term given in Eq. 2.38 and redefines it as given in Eq. 2.103.

$$(\nu \Delta(\mathbf{v}))_i = \sum_j m_j \frac{2(\nu_i + \nu_j)}{\rho_i + \rho_j} \frac{\mathbf{v}_{ij} \mathbf{r}_{ij} \cdot \nabla_i W_{h,ij}}{|\mathbf{r}_{ij}|^2} \quad (2.103)$$

The author tested the model on the problem of 2D wave breaking and overtopping of a sloping wall and compared the results obtained against experimental data (T. Li, Troch, and De Rouck 2004) to validate the model—the computational domain of $\approx 6 \times 10^3$ particles.

As seen from the evolution of the water surface elevation plotted in Fig. 2.19, the author could ascertain that the proposed model produced better results than those of Li et al. (T. Li, Troch, and De Rouck 2004), compared to the experimental data in Fig. 2.19(a) and Fig. 2.19(b). This could be attributed to the free surfaces being accurately tracked by particles without numerical diffusion. In Fig. 2.19(c) and Fig. 2.19(d), despite the wave profiles being consistent with each other in phase and shape, the proposed model predicts smaller elevation levels. Li et al. use a dynamic Smagorinsky model, whereas the proposed model uses constant empirical coefficients. The author believes these coefficients derived from a quasi-steady state may behave sub-optimally in transient flow, such as the problem at hand.

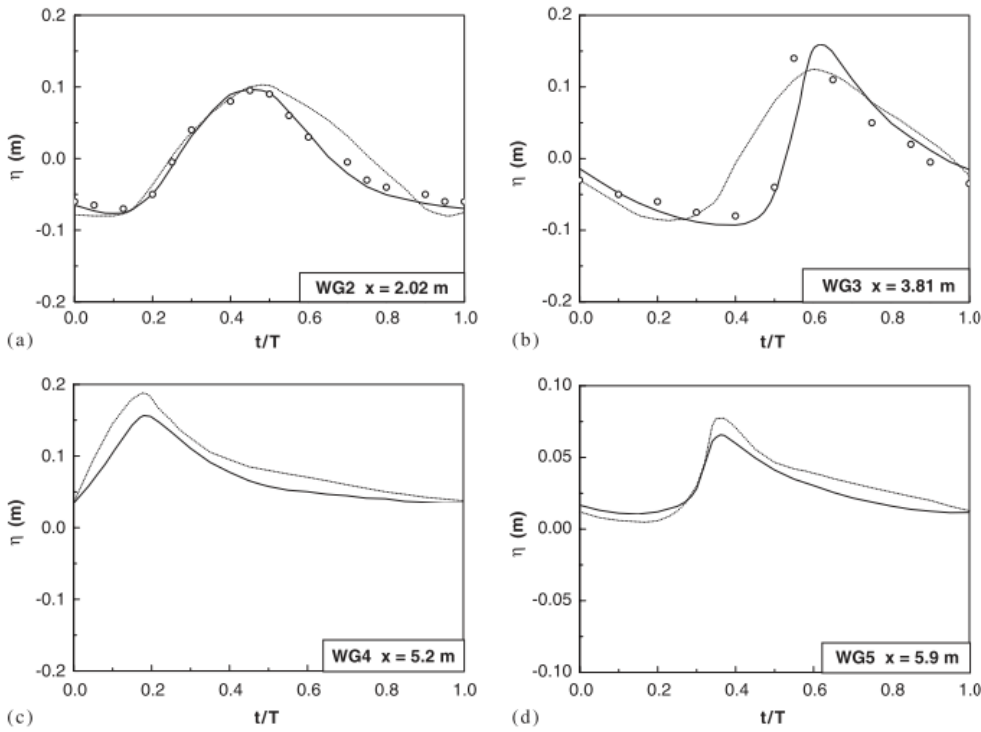


Figure 2.19: Comparisons of computed water surface elevations by SPH (solid lines) with experimental (○) and numerical (dotted lines) data of Li et al. (T. Li, Troch, and De Rouck 2004). Reproduced from Songdong Shao 2006

The author concludes that the $k - \epsilon$ model would require further sensitivity analysis for the turbulence model and spatial resolution for improved results, despite being reasonably accurate in tracking free surfaces.

Wang and Liu (Wang and P. L. Liu 2020) build on the work of Shao (Songdong Shao 2006) to further improve the ISPH $k - \epsilon$ model. They achieved this by using the modelling and computational developments which SPH has benefited from since the work of Shao. The authors here consider the same SPH discretised equations and two-step time integrator as Shao, with two distinct modifications in the Pressure Poisson equation as given by Eq. 2.104 instead of Eq. 2.30. They also redefined propagation equation for (\mathbf{r} using Eq. 2.105 instead of Eq. 2.32.

$$\nabla \cdot \left(\frac{1}{\rho_o} \nabla P_{t+1} \right) = \frac{1}{\Delta t} \nabla \cdot \mathbf{u}_* \quad (2.104)$$

$$\mathbf{r}_{t+1} = \mathbf{r}_* + \Delta \mathbf{v}_{**} \Delta t \quad (2.105)$$

The authors also provided SPH discretization for the transport equations for (k) and (ϵ) using Eq. 2.107 and Eq. 2.108 which requires the use of particle density (φ) as given in Eq. 2.106.

$$\varphi_i = \sum_j W_{h,ij} \quad (2.106)$$

$$\nabla \cdot \left(\frac{\nu_t}{\sigma_k} \nabla k \right)_i = - \sum_j \frac{1}{\varphi_j} \left(\frac{\nu_{t,i}}{\sigma_k} + \frac{\nu_{t,i}}{\sigma_k} \right) \frac{k_{ij} \mathbf{r}_{ij} \nabla_i W_{h,ij}}{|\mathbf{r}_{ij}|^2} \quad (2.107)$$

$$\nabla \cdot \left(\frac{\nu_t}{\sigma_\epsilon} \nabla \epsilon \right)_i = - \sum_j \frac{1}{\varphi_j} \left(\frac{\nu_{t,i}}{\sigma_\epsilon} + \frac{\nu_{t,i}}{\sigma_\epsilon} \right) \frac{\epsilon_{ij} \mathbf{r}_{ij} \nabla_i W_{h,ij}}{|\mathbf{r}_{ij}|^2} \quad (2.108)$$

The authors also derived an SPH formulation for the strain rate tensor defined in Eq. 2.109, which is based on the studies done on kernel correction (Bonet and Lok 1999; Khayyer, Gotoh, and SD Shao 2008) and given by Eq. 2.110 and Eq. 2.111.

$$\underline{S}_i = \frac{1}{2} \left(\nabla \mathbf{v}_i + (\nabla \mathbf{v}_i)^T \right) \quad (2.109)$$

$$\nabla \mathbf{v}_i = - \sum_j \frac{1}{\varphi_j} \mathbf{v}_{ij} \otimes \underline{L}_i \nabla_i W_{h,ij} \quad (2.110)$$

$$\underline{L}_i = \left(- \sum_j \frac{1}{\varphi_j} \nabla_i W_{h,ij} \otimes \mathbf{r}_{ij} \right)^{-1} \quad (2.111)$$

The authors validated the model against the problem of a solitary wave propagating over a bottom-mounted barrier in 2D. Its results are shown in Fig. 2.20. They also considered the problem involving wave breaking on a slopping wall in 2D, which is shown in Fig. 2.21.

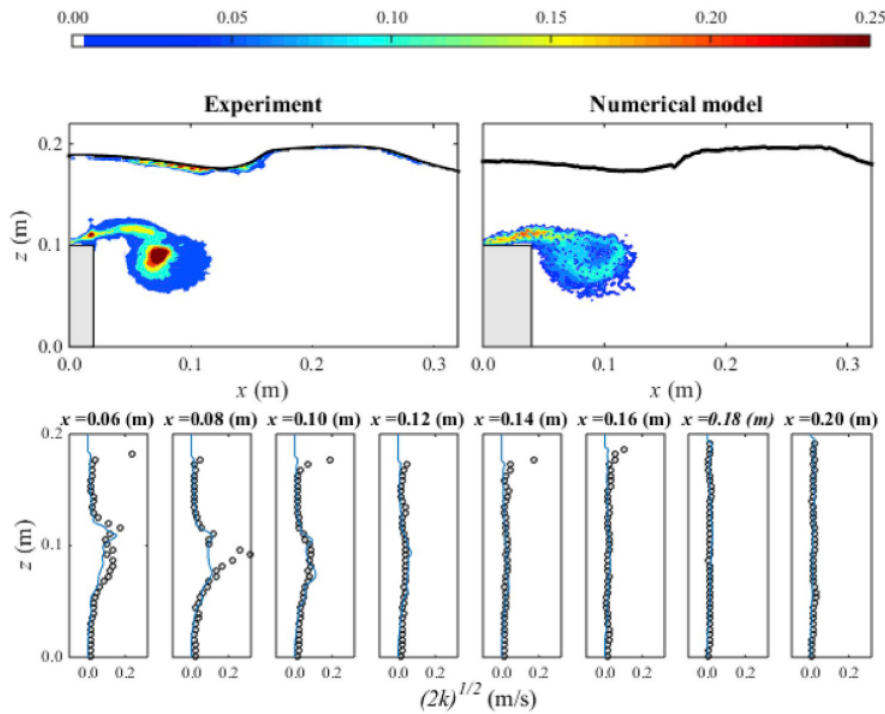


Figure 2.20: Comparisons between experimental data (left) and numerical results (right) for turbulence intensity (m/s) at $t = 0.6s$ (top panels) and the corresponding vertical cross-sections (lower panels). In the lower panels, solid lines and \circ represent the numerical and experimental results, respectively. Reproduced from Wang and P. L. Liu 2020

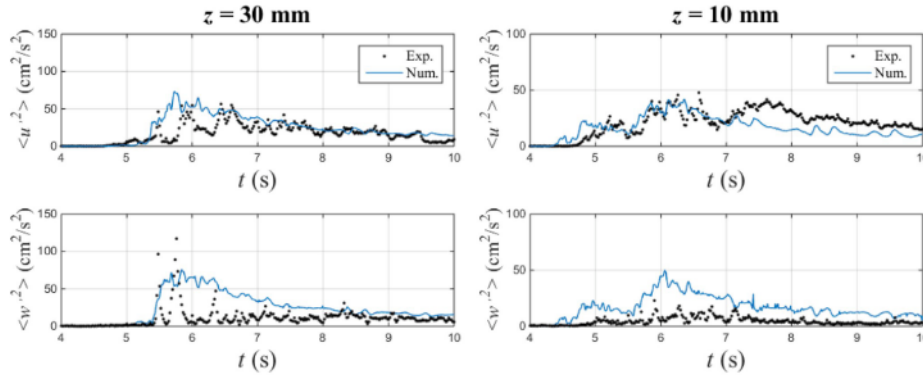


Figure 2.21: Comparisons of numerical and experimental turbulent kinetic energy in x-direction and y-direction. Reproduced from Wang and P. L. Liu 2020

Given the model's accuracy, as observed from the figures, the authors conclude that the model's capabilities have been demonstrated, especially in tracking transient-free surfaces. They also reproduce the evolution of turbulence and its intensity due to flow separation. However, they note that the model under-predicts the max turbulent kinetic energy and is sensitive to the initial seeding of the turbulent kinetic energy property. The authors also state that the counteracting effects of the physical viscous dissipation and numerical dissipation, dependent on the particle resolution, would have to be appropriately balanced. Finally, the authors conclude on the importance of boundary treatment and the need for more sophisticated boundary models to extend the model to 3D domains.

2.5 LANS-based Models

So far, having dealt with RANS and LES models of turbulence, a few fundamental drawbacks of these techniques have been brought to light. In the case of RANS, the flow field is decomposed into an averaged mean flow and a fluctuating field. Such a decomposition of the NS equations provides differential equations for the mean flow containing contributions from the time-varying turbulent motion. Therefore a closure model is required to capture the effects of the fluctuations on the mean flow. However, by studying only the mean flow quantities, the complete nature of the flow, notwithstanding the complex structures stemming from these fluctuations, cannot be studied, let alone appreciated.

On the face of it, LES would have made for a reasonable alternative to model turbulent flows. This is because the large scales in the flow are resolved by the standard NS equations, while the effects of smaller scales are modelled. However, this remains easier said than done since inhomogeneous and wall-bounded flows necessitate the LES filter width to vary dynamically to capture the average size of turbulent eddies.

The other widespread method of tackling turbulence involves Direct Numerical Simulation (DNS). However, since the number of degrees of freedom for a 3D flow grows rapidly with the Reynolds number ($\propto Re^{9/4}$), this technique effectively places an inviolable upper bound on the Re for a given simulation because of computational limitations.

In order to tackle the issues above and address them reasonably, we look for possible solutions. One such solution is the Lagrangian averaging method introduced

by Holm et al. (Holm, Jerrold E Marsden, and Ratiu 1998) and Marsden and Shkoller (J. E. Marsden and Shkoller 2001). In this method, unlike the averaging or filtering of the NS equations as done in RANS or LES, the Lagrangian averaging approach averages at the level of the variational principle from which the Navier–Stokes equations are derived. This procedure yields the Lagrangian-averaged Navier Stokes- α (LANS- α) equations, which describe the time evolution of large eddies in turbulent flows. It can be stated that this approach is similar to that of LES.

The LANS- α equations, assuming incompressibility and isotropic turbulence, are derived and simplified by Mohseni et al. (Mohseni et al. 2003). These equations are as follows:

$$\nabla \cdot \mathbf{v} = 0 \quad (2.112)$$

$$\frac{D\mathbf{v}}{Dt} = \underline{\sigma}(\mathbf{v}) \quad (2.113)$$

$$\underline{\sigma}(\mathbf{v}) = -P\underline{\mathbf{I}} + 2\nu(1 - \alpha^2\Delta)\underline{\mathbf{S}} + 2\alpha^2\underline{\dot{\mathbf{S}}} \quad (2.114)$$

$$\dot{\underline{\mathbf{S}}} = \frac{D\underline{\mathbf{S}}}{Dt} + \underline{\mathbf{SR}} - \underline{\mathbf{RS}} \quad (2.115)$$

$$\underline{\mathbf{R}} = \frac{1}{2} \left(\nabla \mathbf{v} - (\nabla \mathbf{v})^T \right) \quad (2.116)$$

Where α denotes the scale of rapid fluctuations in the flow map, such that for scales smaller than α , the wave activity is filtered by a nonlinear energy redistribution. Here, $(1 - \alpha^2\Delta)$ denotes the Helmholtz operator.

Monaghan (J. J. Monaghan 2002), building on the work of Holm (Holm, Jerrold E Marsden, and Ratiu 1998), attempted to formulate an SPH version of the continuum LANS- α equations. His work provided one of the earliest models of turbulence in compressible flow. The author incorporated some of his earlier work on XSPH (J. Monaghan 1989), in which particles are moved with a smoothed velocity, leaving the acceleration equation unchanged. The smoothed velocity denoted an average over the velocities of the neighbouring particles. This facilitated the author in writing the Lagrangian analysed by Holm in an SPH form, allowing for the subsequent derivation of the momentum equation, albeit being elaborate and highly complicated. Nevertheless, in conjunction with the continuity equation, the derived momentum equation formulated the SPH- α model, which essentially consisted of an SPH particle moving with the transport velocity smoothed from momentum velocity by an iterative algorithm with an additional dissipation term meant to mimic the standard LES model.

Hu and Adams (X. Y. Hu and N. A. Adams 2015) also devised a turbulence model for incompressible flow based on spatial filtering of the NS equations using SPH approximations termed the SPH- σ model. The model shares similarities with the LANS- α model and the SPH- α model, differing by the additional stress term in the model and its approach in evaluating the particle transport velocity. The proposed model is also built on the authors' previous work (X. Hu and Nikolaus A Adams 2007), and hence shares similar numerical techniques. The authors also validated the proposed model on 2D flow comprising decaying and forced turbulence cases. Their results suggested that the model could simulate incompressible turbulent flow.

Monaghan (J. J. Monaghan 2011, 2017) subsequently improved on the SPH- α model and derived a more amenable variant of the momentum equation. Since, in this case, the model was parameterised around the smoothing parameter (ϵ), the turbulence model was termed the SPH- ϵ model. The linearly smoothed velocity ($\hat{\mathbf{v}}$)

is given by Eq. 2.117.

$$\hat{\mathbf{v}}_i = \mathbf{v}_i - \varepsilon \sum_j \frac{m_j}{M_o} \mathbf{v}_{ij} K_{h',ij} \quad , \quad \varepsilon \in [0, 1] \quad (2.117)$$

Where (K) is a smoothing kernel, which can be different from the kernel used in SPH, its corresponding smoothing length being (h'). It is noted that the smoothed velocity preserves the shape of the spectrum of the unsmoothed velocity for short-length scales. However, it reduces the magnitude of the unsmoothed velocity by a factor ($1 - \varepsilon$).

The equation of state is given by Eq. 2.1, and the momentum equation is given by Eq. 2.118. The momentum equation's third term on the right-hand side is an extra stress term determined by the smoothing. Its overall effect is to redistribute energy without dissipation.

$$\frac{D\mathbf{v}_i}{Dt} = - \sum_j m_j \left(\frac{P_i}{\rho_i^2} + \frac{P_j}{\rho_j^2} \right) \nabla_i W_{h,ij} - \sum_j m_j \Pi_{ij} \nabla_i W_{h,ij} + \frac{\varepsilon}{2} \sum_j \frac{m_j}{M_o} |\mathbf{v}_{ij}| \nabla_i W_{h,ij} \quad (2.118)$$

Where the viscosity term (Π_{ij}) is given by Eq. 2.119, in which (α) is a constant.

$$\Pi_{ij} = - \frac{2\alpha c_s \mathbf{v}_{ij} \cdot \mathbf{r}_{ij}}{(\rho_i + \rho_j) |\mathbf{r}_{ij}|^2} \quad (2.119)$$

The particles are subsequently transported using Eq. 2.120.

$$\frac{D\mathbf{r}_i}{Dt} = \hat{\mathbf{v}}_i \quad (2.120)$$

The author validated the proposed model by simulating 2D flow past a cylinder moving along a Lissajous curve. The author demonstrated the model's capabilities to predict satisfactory results for the velocity correlation functions, energy spectrum and mixing while having particle resolution be half of that required for a DNS with a resolution the Reynolds length. The author concludes that the model's effectiveness for higher Reynolds numbers and other boundary conditions, such as free surfaces, will need to be studied further.

2.6 Miscellaneous Models

Liu et al. (S. Liu et al. 2019) approach the problem of turbulence modelling from the perspective of computer 3D visualisation to visualise flows with realistic features. The authors' viscosity-based vorticity correction model offers more advantages to the computer visual-effects audience. However, the model would still be a worthwhile investigation.

The authors define a vorticity field (ω) in the system as given in Eq. 2.121.

$$\boldsymbol{\omega}_i = \nabla \times \mathbf{v}_i = - \frac{1}{\rho} \sum_j m_j \mathbf{v}_{ij} \times \nabla_i W_{h,ij} \quad (2.121)$$

The contribution to the SPH particle's momentum velocity from the viscous term is calculated as given in Eq. 2.122.

$$\mathbf{v}_{v,i} = \mathbf{v}_i + \mathbf{a}_i^{(visc)} \Delta t \quad (2.122)$$

If the magnitude of viscous velocity ($\mathbf{v}_{v,i}$) is greater than (\mathbf{v}_i) for a given particle, then its vorticity field is updated as given in Eq. 2.123.

$$\delta\omega_i = (\alpha\sqrt{R_i})\omega_i \quad (2.123)$$

$$R_i = \frac{\delta E_i}{E_i} = \frac{\mathbf{v}_{v,i}^2 - \mathbf{v}_i^2}{\mathbf{v}_i^2} \quad (2.124)$$

A stream function (Ψ) is subsequently defined as given in Eq. 2.125.

$$\Psi_i = \sum_j \frac{\delta\omega_j \mathcal{V}_j}{4\pi |\mathbf{r}_{ij}|} \quad (2.125)$$

The velocity correction ($\delta\mathbf{v}$) for the particle is subsequently defined by Eq. 2.126.

$$\delta\mathbf{v}_i = \nabla \times \Psi_i \quad (2.126)$$

Obeidat and Bordas (Obeidat and Bordas 2018), tackle the problem of turbulence by devising a hybrid remeshed method (hrSPH) for the simulation of three-dimensional turbulent flows. The authors essentially use an Eulerian mesh with Lagrangian particles to gain advantages of both schemes. The governing equations are evaluated using the properties at the mesh nodes, which are interpolated from the particles. After evaluating the system of equations, the new properties on the mesh nodes are used to update the properties of the particles through mesh-to-particle interpolation. The authors consider the turbulent sub-grid stresses using the Smagorinsky model.

The proposed model remeshes the particles when the distribution is not uniform. The authors validated the model against the 2D and 3D TGV problems, thin double shear layer problems, and 3D isotropic turbulence obtained from DNS. The model predicts the energy spectra and energy dissipation reasonably well. Despite the model's accuracy, not much information can be gathered to help solely improve the state of turbulence modelling in SPH.

3 Evaluation of Turbulence Models

Turbulence, as a phenomenon, has been notoriously difficult for a detailed physical analysis. This is further exacerbated by the seemingly endless complex interactions it gives rise to in the flow as long as any form of energy is provided. Therefore, while modelling turbulence remains one facet of the problem, visualising and analysing the model is another equally challenging task.

As seen in the previous [Chapter 2](#), numerous Lagrangian turbulent models seem to be tested for only complex surface flows. However, a systematic analysis of isotropic turbulence problems provides greater insight into the energy spectrum and its corresponding cascade across varying length scales. A reasonable model should be able to capture the characteristic hierarchy of scales through which the energy cascade takes place. The dissipation of kinetic energy finally occurs at the scales of the order of Kolmogorov length, where the flow subsequently becomes laminar. In contrast, the injection of energy in turbulent flow generally occurs at much larger scales.

Hence, appropriate test cases must be used when analysing turbulence.

3.1 Benchmark Problems

3.1.1 Taylor-Green Vortex Problem

The Taylor-Green vortex problem is a challenging case to tackle. The flow is periodic, incompressible and consists of decaying vortices. The 2D case of the problem is analytically defined as given by [Eq. 3.1](#) - [Eq. 3.3](#).

$$v_x = -Ue^{bt} \cos(2\pi x) \sin(2\pi y) \quad (3.1)$$

$$v_y = Ue^{bt} \sin(2\pi x) \cos(2\pi y) \quad (3.2)$$

$$p = (Ue^{bt})^2 \frac{\cos(4\pi x) + \cos(4\pi y)}{4} \quad (3.3)$$

$$b = -\frac{8\pi}{Re} \quad , \quad Re = \frac{UL}{\nu} \quad (3.4)$$

Where (U, Re, L) are flow constants.

The 3D case of the problem, defined for a tri-periodic domain with boundary $(\Omega = [0, 2\pi]^3)$ is initially set-up as given in [Eq. 3.5](#) - [Eq. 3.7](#).

$$v_{x,0} = \sin(x) \cos(y) \cos(z) \quad (3.5)$$

$$v_{y,0} = -\cos(x) \sin(y) \cos(z) \quad (3.6)$$

$$v_{z,0} = 0 \quad (3.7)$$

The corresponding initial pressure field (P_0) obtained from solving the pressure Poisson equation for incompressible flow is given by Eq. 3.8 (Pereira et al. 2021).

$$P_0 = P_o + \frac{\rho_o v_o^2}{16} \left(2 + \cos(2z) \right) \left(\cos(2x) + \cos(2y) \right) \quad (3.8)$$

3.1.2 Thin Double-Shear Layer

The thin double-shear layer is a problem often considered to be too difficult to simulate due to the small scales which are produced. The main challenge of the problem, as shown by Brown and Minion (Minion and Brown 1997), occurs when a numerical method produces spurious structures, especially when the flow is sufficiently under-resolved. Drikakis and Smolarkiewicz (Drikakis and Smolarkiewicz 2001) studied the problem's spurious structure to understand its numerical mechanism. They indicated that the spurious structure's generation depends on the advective scheme's choice.

The initial conditions for the 2D periodic flow is given by Eq. 3.9 - Eq. 3.10.

$$v_{x,0} = \tanh(80 \times \min[y - 0.25, 0.75 - y]) \quad (3.9)$$

$$v_{y,0} = \delta \sin(2\pi(x + 0.25)) \quad (3.10)$$

3.1.3 3D Isotropic Turbulence

The JHU Turbulence Database Cluster (Y. Li et al. 2008) provide a direct numerical simulation (DNS) data set for isotropic, forced turbulence. The data set consists of the DNS output on 1024^3 spatial points and 1024 time samples spanning about one large-scale turnover time.

The entire 1024^4 space-time history of the incompressible DNS simulation ($Re \approx 1460$) is accessible to users remotely through an interface based on the Web-services model. The data from the database contains the three velocity components and the pressure. A uniform non-dimensionalised pressure ($P^* = \frac{P}{\rho U^2} + 1$) is added to the database pressure, with Mach number Ma 0.1.

3.1.4 2D Confined & Driven Turbulence

Based on the test case employed by Monaghan (J. J. Monaghan 2017), a 2D fluid confined to a square solid impenetrable boundary is considered ($\Omega = [0, 1]^2$). A cylinder of radius ($r = 0.7$) is placed at the centre of the box. The circle is subsequently provided with a Lissajous trajectory to follow given by Eq. 3.11 - Eq. 3.12.

$$x = 0.5 + 0.25 \sin\left(\frac{2\pi t}{5}\right) \quad (3.11)$$

$$y = 0.5 + 0.25 \sin\left(\frac{4\pi t}{5}\right) \quad (3.12)$$

3.1.5 Free Surface Flows

As seen in numerous works involving turbulence models in the previous chapter, there does not appear to be any dearth of experimental and numerical research on free-surface flows. Problems ranging from the classic 2D and 3D dam break to wave

propagation, wave breaking, water overtopping, and dyke-flow inspired problems can be simulated. The only caveat involved in such cases includes the resolution requirements of the problem and the approach taken in free surfaces boundary condition implementation.

3.2 Post-Simulation Analysis

3.2.1 Energy Spectral Density

In order to analyse the predicted flow and validate the turbulent model, energy spectra are the most used description since it has to fall off as prescribed by the Kolmogorov - 5/3 Law. Typical mesh or grid-based methods facilitate the calculation of the energy spectrum ($E[\mathbf{k}]$) by using the Fourier transform of the velocity field as given in Eq. 3.13, to obtain the velocity spectrum as defined in Eq. 3.14.

$$\mathbf{V}(\mathbf{k}) = \frac{1}{L^3} \int \exp(-i\mathbf{k} \cdot \mathbf{r}) \mathbf{v}(\mathbf{r}) d\mathbf{r} \quad (3.13)$$

Where ($d\mathbf{r} = dx dy$) for 2D and ($d\mathbf{r} = dx dy dz$) for 3D, and [$\mathbf{k} = (k_x, k_y, k_z)$] is the wave-number vector.

$$E(\mathbf{k}) = \frac{1}{2} |\mathbf{V}(\mathbf{k}) \cdot \mathbf{V}^*(\mathbf{k})| \quad (3.14)$$

The energy spectrum is subsequently defined as given by Eq. 3.15 for the case of isotropic turbulence.

$$E(\mathbf{k}) = B \langle E(\mathbf{k}) \rangle, \quad k = |\mathbf{k}| \quad (3.15)$$

Where ($B = 2\pi k$) for 2D and ($B = 4\pi k^2$) for 3D.

However, SPH does not have such grid-like data to calculate the energy spectrum directly. Hence, the data has to be reconstructed using interpolation methods as outlined by Shi et al. (Shi et al. 2013). The authors provide three distinct methods of interpolating the data across a grid-like space. The SPH interpolation method specified by the authors is given in Eq. 3.16.

$$A(\mathbf{r}) \approx \sum_j A_j W(|\mathbf{r} - \mathbf{r}_j|, h) \mathcal{V}_j \quad (3.16)$$

The remeshed interpolation method is outlined in Eq. 3.17. Remeshed Interpolation

$$A(\mathbf{r}) \approx \sum_j A_j \tilde{W}(|x - x_j|, h) \tilde{W}(|y - y_j|, h) \tilde{W}(|z - z_j|, h) \quad (3.17)$$

Where (\tilde{W}) represents the kernel where the volume of the particle (\mathcal{V}_j) has been absorbed.

The authors also detail the moving least squares (MLS) method as an interpolation tool. Building on the work of Lancaster and Salkauskas (Lancaster and Salkauskas 1981), who were able to extend the 2D interpolation technique proposed by Shepard (Shepard 1968) to a general higher-order case. The authors state that they start with a weighted least squares formulation for an arbitrary fixed point and then move said point across the entire domain. This allows for the computation of a weighted least squares fit function, which can be used to evaluate grid-like points.

3.2.2 Lagrangian Coherent Structures

Complex flow cannot only be analysed through primitive flow properties such as pressure, velocity or energy density for a deep understanding of the flow interactions. Techniques using only such properties would fail to identify general coherent structures (CS) in the flow. To facilitate that, quantities such as those employing the velocity gradient, such as the vorticity, Q-criterion, Δ -criterion, swirling strength criterion, etc., are used. However, Haller (Haller 2005) was able to show that in some situations, most of the definitions of the vortex are not objective and suitable for studying the flow, particularly in the context of 3D flow.

Therefore, Sun et al. (Sun, Colagrossi, et al. 2016) utilise the Lagrangian Coherent Structures (LCSs) as an alternative way with specific advantages for drawing the CSs from a given flow field. In order to identify the LCSs with an objective quantity, the authors use the Finite-time Lyapunov Exponent (FTLE), which represents the rate of separation of the nearby fluid particles over a finite time interval. FTLEs can be evaluated both in forward and backward time directions.

The authors summarise the main advantages of FTLEs over different velocity gradient-based metrics as follows:

- Local fluctuations of the velocity field do not induce noise to FTLEs since they are integrated in time.
- FTLE is formulated in the Lagrangian frameworks allowing for better identification of the LCSs with respect to quantities derived from the velocity gradient.
- FTLE can identify LCSs with an accuracy that, in some cases, resemble those obtained from advanced experimental techniques.

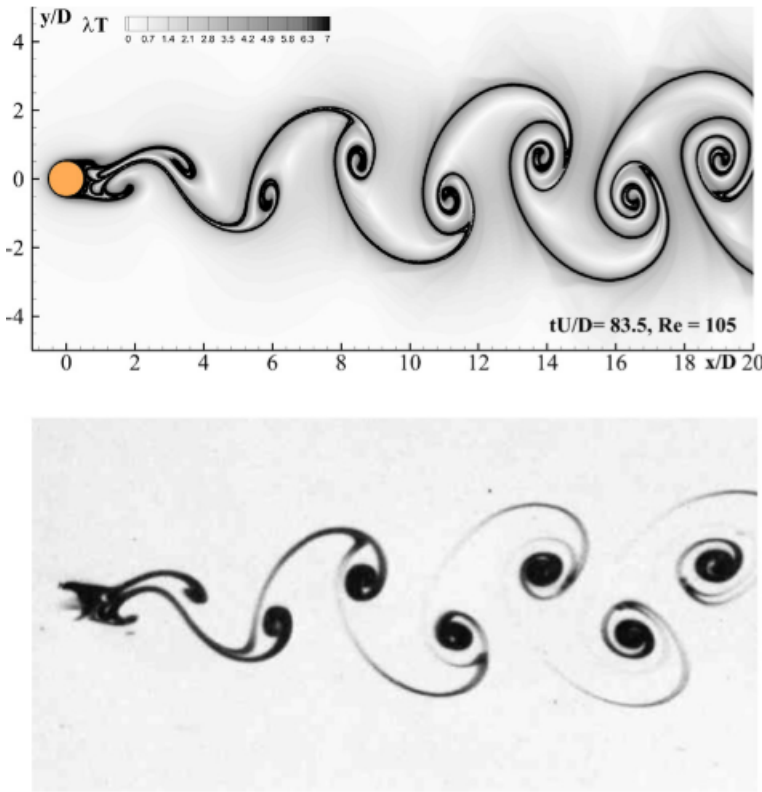


Figure 3.1: Viscous flow past a circular cylinder at $Re = 105$. Top: Attracting FTLE contour plot from SPH simulation. Bottom: Photo from experiments conducted by Taneda (Taneda 1977) with electrolytic precipitation in water technique for vortex street visualisation. Reproduced from Sun, Colagrossi, et al. 2016

The forward-in-time FTLE is calculated using the forward-in-time Right-Cauchy-Green strain tensor, while backward-in-time FTLE requires the Left-Cauchy-Green strain tensor. The authors propose two methods to calculate a flow's Cauchy-Green strain tensors.

The first method uses SPH formulations for the deformation gradient to compute the Cauchy-Green strain tensors. The backward-in-time FTLE can be computed using limited resources during run-time concurrently in this method. However, the forward-in-time FTLE can only be computed during post-processing.

In the second method, the forward-in-time deformation gradient is evolved as a property within the simulation's time integration step employing a governing equation for the property. This method does not need to keep track of the spatial relation between the points. This allows for the process to be suitable for Eulerian solvers as well. Building on this work, Dauch et al. (Dauch et al. 2018) developed an efficient GPU-based implementation to accelerate the computation of FTLE fields or, depending on the architecture of the solver, completely move the step from being calculated on the CPU to the GPU. Their proposition is highly enticing, especially for 3D flows.

4 Conclusion & Future Work

Werner Heisenberg, an eminent theoretical physicist of the 20th century and one of the pioneers of quantum mechanics, said -

"When I meet God, I am going to ask him two questions: why relativity? And why turbulence? I really believe he will have an answer for the first."

His tongue-in-cheek quip regarding turbulence seems relevant even today, given that the comprehensive theory of turbulence still eludes us. This is a testament to the complexity of dealing with turbulence from a theoretical and numerical perspective.

At the interim stage of this project, a reasonable database of past SPH turbulence models has been compiled, with their corresponding advantages, limitations and potential areas for refinement. Efforts to extend the EDAC scheme (Ramachandran and Puri 2019) with the Lagrangian LES model is rendered challenging as detailed in Sec. 2.3.1. The scheme also cannot make use of RANS-based models since the averaging technique assumes incompressibility, which simplifies to $(\nabla \cdot \mathbf{v} = 0)$, which would affect the transport equation for pressure Eq. 2.94 which contains a term dependent of the divergence of velocity. It is, therefore, worthwhile to consider the compressible form of EDAC (Chola and Shintake 2021) and proceed to develop a suitable turbulence for the scheme. This would be a fruitful endeavour since the scheme typically produces a smoother and more accurate pressure distribution for flows, confined or free, without requiring artificial viscosity.

Subsequently, once a class of well-equipped turbulent models have been identified, it is intended to use those models in conjunction with a second-order convergent scheme of SPH, such as the L-IPST-C scheme devised by Negi and Ramachandran (Negi and Ramachandran 2022).

Following that, the subsequent stage of the project can delve into incorporating adaptive particle refinement to reduce the computational cost for the flow simulation for a given quality of the solution. Work done by Muta and Ramachandran (Muta and Ramachandran 2022) will be considered to make this concept of "adaptive turbulence" modelling feasible.

Achieving these objectives would allow work to be done on incorporating boundary conditions and wall functions for turbulence modelling as detailed by Mayrhofer (Arno Mayrhofer 2014). This would therefore allow for simulations involving moving or deformable geometries, in which case the issue of the computational cost would take precedence. The work of Haftu et al. (Haftu, Muta, and Ramachandran 2022) on parallel adaptive WCSPH and Negi et al. (Negi, Ramachandran, and Haftu 2020) on inlet-outlet boundary conditions would serve as a helpful junction to proceed in future.

A Lagrangian LES Filtering of EDAC

EDAC Pressure evolution equation:

$$\frac{D P}{D t} = -c_s^2 \rho \nabla \cdot \mathbf{v} + \nu \nabla^2 P \quad (\text{A.1})$$

Lagrangian LES filter (Di Mascio et al. 2017):

$$\phi = \phi(\tilde{\mathbf{r}}_p(t) - \mathbf{y}, t - \tau) \quad (\text{A.2})$$

Substituting Eq. A.2 in Eq. A.1

$$\tilde{P}(\tilde{\mathbf{r}}_p, t) = \int_{\mathbb{R}^3} \int_{-\infty}^{\infty} \phi(\tilde{\mathbf{r}}_p(t) - \mathbf{y}, t - \tau) P(\mathbf{y}, \tau) d\tau dV_y \quad (\text{A.3})$$

Applying the Lagrangian derivative operator on both sides

$$\frac{D \tilde{P}(\tilde{\mathbf{r}}_p, t)}{D t} = \frac{D}{D t} \left(\int_{\mathbb{R}^3} \int_{-\infty}^{\infty} \phi(\tilde{\mathbf{r}}_p(t) - \mathbf{y}, t - \tau) P(\mathbf{y}, \tau) d\tau dV_y \right) \quad (\text{A.4})$$

Commuting the Lagrangian derivative operator and the integral operator

$$\frac{D \tilde{P}(\tilde{\mathbf{r}}_p, t)}{D t} = \int_{\mathbb{R}^3} \int_{-\infty}^{\infty} \frac{D \left(\phi(\tilde{\mathbf{r}}_p(t) - \mathbf{y}, t - \tau) P(\mathbf{y}, \tau) \right)}{D t} d\tau dV_y \quad (\text{A.5})$$

Applying chain rule and introducing $(\mathcal{I}_1, \mathcal{I}_2)$

$$\begin{aligned} \frac{D \tilde{P}(\tilde{\mathbf{r}}_p, t)}{D t} &= \int_{\mathbb{R}^3} \int_{-\infty}^{\infty} \left(\frac{\partial \phi(\tilde{\mathbf{r}}_p(t) - \mathbf{y}, t - \tau)}{\partial t} + \frac{D \tilde{\mathbf{r}}_p}{D t} \cdot \nabla \phi(\tilde{\mathbf{r}}_p(t) - \mathbf{y}, t - \tau) \right) P(\mathbf{y}, \tau) d\tau dV_y \\ &= \int_{\mathbb{R}^3} \int_{-\infty}^{\infty} \left(\underbrace{\frac{\partial \phi(\tilde{\mathbf{r}}_p(t) - \mathbf{y}, t - \tau)}{\partial t}}_{\mathcal{I}_1} + \underbrace{\tilde{\mathbf{v}}(\tilde{\mathbf{r}}_p, t) \cdot \nabla \phi(\tilde{\mathbf{r}}_p(t) - \mathbf{y}, t - \tau)}_{\mathcal{I}_2} \right) P(\mathbf{y}, \tau) d\tau dV_y \\ &= \int_{\mathbb{R}^3} \int_{-\infty}^{\infty} (\mathcal{I}_1 + \mathcal{I}_2) P(\mathbf{y}, \tau) d\tau dV_y \end{aligned} \quad (\text{A.6})$$

Rewriting (\mathcal{I}_1) as a function of $[\phi(\tilde{\mathbf{r}}_p(t) - \mathbf{y}, t - \tau)]$ using integration by parts

$$\begin{aligned} \int_{\mathbb{R}^3} \int_{-\infty}^{\infty} \mathcal{I}_1 P(\mathbf{y}, \tau) d\tau dV_y &= \int_{\mathbb{R}^3} \int_{-\infty}^{\infty} \frac{\partial \phi(\tilde{\mathbf{r}}_p(t) - \mathbf{y}, t - \tau)}{\partial t} P(\mathbf{y}, \tau) d\tau dV_y = \\ &\quad \int_{\mathbb{R}^3} \int_{-\infty}^{\infty} \phi(\tilde{\mathbf{r}}_p(t) - \mathbf{y}, t - \tau) \frac{\partial P(\mathbf{y}, \tau)}{\partial \tau} d\tau dV_y \end{aligned} \quad (\text{A.7})$$

Rewriting (\mathcal{I}_2) as a function of $[\phi(\tilde{\mathbf{r}}_p(t) - \mathbf{y}, t - \tau)]$ using integration by parts

$$\int_{\mathbb{R}^3} \int_{-\infty}^{\infty} \mathcal{I}_2 P(\mathbf{y}, \tau) d\tau dV_y = \int_{\mathbb{R}^3} \int_{-\infty}^{\infty} \left(\tilde{\mathbf{v}}(\tilde{\mathbf{r}}_p, t) \cdot \nabla \phi(\tilde{\mathbf{r}}_p(t) - \mathbf{y}, t - \tau) \right) P(\mathbf{y}, \tau) d\tau dV_y = \\ \int_{\mathbb{R}^3} \int_{-\infty}^{\infty} \phi(\tilde{\mathbf{r}}_p(t) - \mathbf{y}, t - \tau) \tilde{\mathbf{v}}(\tilde{\mathbf{r}}_p, t) \cdot \nabla_y P(\mathbf{y}, \tau) d\tau dV_y \quad (\text{A.8})$$

Substituting Eq. A.7 and Eq. A.8 in Eq. A.6 and introducing (\mathcal{I})

$$\frac{D \tilde{P}(\tilde{\mathbf{r}}_p, t)}{Dt} = \int_{\mathbb{R}^3} \int_{-\infty}^{\infty} \phi(\tilde{\mathbf{r}}_p(t) - \mathbf{y}, t - \tau) \underbrace{\left(\frac{\partial P(\mathbf{y}, \tau)}{\partial \tau} + \tilde{\mathbf{v}}(\tilde{\mathbf{r}}_p, t) \cdot \nabla_y P(\mathbf{y}, \tau) \right)}_{\mathcal{I}} d\tau dV_y \\ = \int_{\mathbb{R}^3} \int_{-\infty}^{\infty} \phi(\tilde{\mathbf{r}}_p(t) - \mathbf{y}, t - \tau) (\mathcal{I}) d\tau dV_y \quad (\text{A.9})$$

Rewriting (\mathcal{I}) by incorporating Eq. A.1

$$\frac{\partial P(\mathbf{y}, \tau)}{\partial \tau} + \tilde{\mathbf{v}}(\tilde{\mathbf{r}}_p, t) \cdot \nabla_y P(\mathbf{y}, \tau) = \frac{\partial P(\mathbf{y}, \tau)}{\partial \tau} + \left(\tilde{\mathbf{v}}(\tilde{\mathbf{r}}_p, t) - \mathbf{v}(\mathbf{y}, \tau) + \mathbf{v}(\mathbf{y}, \tau) \right) \cdot \nabla_y P(\mathbf{y}, \tau) \\ = \left(\frac{\partial P(\mathbf{y}, \tau)}{\partial \tau} + \mathbf{v}(\mathbf{y}, \tau) \cdot \nabla P(\mathbf{y}, \tau) \right) + \left(\tilde{\mathbf{v}}(\tilde{\mathbf{r}}_p, t) - \mathbf{v}(\mathbf{y}, \tau) \right) \cdot \nabla_y P(\mathbf{y}, \tau) \\ = \frac{D P(\mathbf{y}, \tau)}{D \tau} + \left(\tilde{\mathbf{v}}(\tilde{\mathbf{r}}_p, t) - \mathbf{v}(\mathbf{y}, \tau) \right) \cdot \nabla_y P(\mathbf{y}, \tau) \\ = \left(-c_s^2 \rho \nabla_y \mathbf{v}(\mathbf{y}, \tau) + \nu \nabla_y^2 P(\mathbf{y}, \tau) \right) + \left(\tilde{\mathbf{v}}(\tilde{\mathbf{r}}_p, t) - \mathbf{v}(\mathbf{y}, \tau) \right) \cdot \nabla_y P(\mathbf{y}, \tau) \quad (\text{A.10})$$

Substituting Eq. A.10 in Eq. A.9, and making use of the fact that the differential and spatial filtering operator commute far from the boundaries $[\nabla \tilde{a} = \widetilde{\nabla a}]$ (Di Mascio et al. 2017)

$$\frac{D \tilde{P}(\tilde{\mathbf{r}}_p, t)}{Dt} = \int_{\mathbb{R}^3} \int_{-\infty}^{\infty} \phi(\tilde{\mathbf{r}}_p(t) - \mathbf{y}, t - \tau) (\mathcal{I}) d\tau dV_y \\ = -c_s^2 \rho \widetilde{\nabla \cdot \mathbf{v}} + \nu \widetilde{\nabla^2 P} + \widetilde{\mathbf{v} \cdot \nabla P} - \widetilde{\mathbf{v} \cdot \nabla \cdot \nabla P} \quad (\text{A.11})$$

$$\therefore \frac{D \tilde{P}}{Dt} = -c_s^2 \rho \nabla \cdot \widetilde{\mathbf{v}} + \nu \nabla^2 \widetilde{P} + \widetilde{\mathbf{v} \cdot \nabla P} - \widetilde{\mathbf{v} \cdot \nabla \cdot \nabla P} \quad (\text{A.12})$$

Bibliography

- Adami, S., X. Y. Hu, and N. A. Adams (2012). *Simulating three-dimensional turbulence with SPH*. Lehrstuhl für Aerodynamik.
- Bonet, Javier and T-SL Lok (1999). "Variational and momentum preservation aspects of smooth particle hydrodynamic formulations". In: *Computer Methods in applied mechanics and engineering* 180.1-2, pp. 97–115.
- Canelas, Ricardo B et al. (2016). "Hunting for Lagrangian Coherent Structures : SPH-LES turbulence simulations with Wall-adapting Local Eddy Viscosity (WALE) model". In: *11th SPHERIC* (March 2017). URL: https://www.researchgate.net/publication/315665064_Hunting_for_Lagrangian_Coherent_Structures_SPH_-_LES_turbulence_simulations_with_Wall-adapting_Local_Eddy_Viscosity_WALE_model.
- Chola, Kalale and Tsumoru Shintake (2021). "Generalized entropically damped artificial compressibility for weakly compressible SPH". In: *Computers and Fluids* 229.July, p. 105093. ISSN: 00457930. DOI: 10.1016/j.compfluid.2021.105093. URL: <https://doi.org/10.1016/j.compfluid.2021.105093>.
- Chorin, Alexandre Joel (1968). "Numerical solution of the Navier-Stokes equations". In: *Mathematics of computation* 22.104, pp. 745–762.
- Clausen, Jonathan R. (2013). "Entropically damped form of artificial compressibility for explicit simulation of incompressible flow". In: *Physical Review E - Statistical, Nonlinear, and Soft Matter Physics* 87.1, pp. 1–12. ISSN: 15393755. DOI: 10.1103/PhysRevE.87.013309.
- Cleary, Paul W and Joseph J Monaghan (1999). "Conduction modelling using smoothed particle hydrodynamics". In: *Journal of Computational Physics* 148.1, pp. 227–264.
- Colagrossi, A (2021). "Smoothed particle hydrodynamics method from a large eddy simulation perspective . Generalization to a quasi-Lagrangian model Smoothed particle hydrodynamics method from a large eddy simulation perspective . Generalization to a quasi-Lagrangian model". In: 015102 (December 2020). DOI: 10.1063/5.0034568. URL: <https://doi.org/10.1063/5.0034568>.
- Colagrossi, A. et al. (Nov. 2021). "Da Vinci's observation of turbulence: A French-Italian study aiming at numerically reproducing the physics behind one of his drawings, 500 years later". In: *Physics of Fluids* 33 (11), p. 115122. ISSN: 1070-6631. DOI: 10.1063/5.0070984. URL: <https://aip.scitation.org/doi/10.1063/5.0070984>.
- Cummins, Sharen J and Murray Rudman (1999). "An SPH projection method". In: *Journal of computational physics* 152.2, pp. 584–607.
- Dalrymple, R A and B D Rogers (2006). "Numerical modeling of water waves with the SPH method". In: 53. Favre-Averaging, Sub-Particle Scaling, Shepard Filtering, pp. 141–147. DOI: 10.1016/j.coastaleng.2005.10.004.
- Dauch, TF et al. (2018). "Highly efficient computation of Finite-Time Lyapunov Exponents (FTLE) on GPUs based on three-dimensional SPH datasets". In: *Computers & Fluids* 175, pp. 129–141.

- Di Mascio, A. et al. (2017). "Smoothed particle hydrodynamics method from a large eddy simulation perspective". In: *Physics of Fluids* 29.3. ISSN: 10897666. DOI: 10.1063/1.4978274.
- Drikakis, Dimitris and Piotr K Smolarkiewicz (2001). "On spurious vortical structures". In: *Journal of Computational physics* 172.1, pp. 309–325.
- Frigo, Matteo and Steven G Johnson (2005). "The design and implementation of FFTW3". In: *Proceedings of the IEEE* 93.2, pp. 216–231.
- GOSSLER, ALBERT A (2001). *Moving Least-Squares: a numerical differentiation method for irregularly spaced calculation points*. Tech. rep. Sandia National Lab.(SNL-NM), Albuquerque, NM (United States); Sandia ...
- Gotoh, Hitoshi, Songdong Shao, and Tetsu Memita (2004). "SPH-LES model for numerical investigation of wave interaction with partially immersed breakwater". In: *Coastal Engineering Journal* 46 (1), pp. 39–63. ISSN: 17936292. DOI: 10.1142/S0578563404000872.
- Haftu, Asmelash, Abhinav Muta, and Prabhu Ramachandran (2022). "Parallel adaptive weakly-compressible SPH for complex moving geometries". In: *Computer Physics Communications* 277, p. 108377. ISSN: 00104655. DOI: 10.1016/j.cpc.2022.108377. arXiv: 2201.00514. URL: <https://doi.org/10.1016/j.cpc.2022.108377>.
- Haller, George (2005). "An objective definition of a vortex". In: *Journal of fluid mechanics* 525, pp. 1–26.
- Hardy, Robert J (1982). "Formulas for determining local properties in molecular-dynamics simulations: Shock waves". In: *The Journal of Chemical Physics* 76.1, pp. 622–628.
- Holm, Darryl D, Jerrold E Marsden, and Tudor S Ratiu (1998). "Euler-Poincaré models of ideal fluids with nonlinear dispersion". In: *Physical Review Letters* 80.19, p. 4173.
- Hu, X. Y. and N. A. Adams (2015). "A SPH Model for Incompressible Turbulence". In: *Procedia IUTAM* 18, pp. 66–75. ISSN: 22109838. DOI: 10.1016/j.piutam.2015.11.007. arXiv: 1204.5097.
- Hu, Xiang Yu and Nikolaus A Adams (2006). "A multi-phase SPH method for macroscopic and mesoscopic flows". In: *Journal of Computational Physics* 213.2, pp. 844–861.
- Hu, XY and Nikolaus A Adams (2007). "An incompressible multi-phase SPH method". In: *Journal of computational physics* 227.1, pp. 264–278.
- Khayyer, A, H Gotoh, and SD Shao (2008). "Corrected incompressible SPH method for accurate water-surface tracking in breaking waves". In: *Coastal Engineering* 55.3, pp. 236–250.
- Kubo, Hidehito and Tsuguo Sunamura (2001). "Large-scale turbulence to facilitate sediment motion under spilling breakers". In: *Coastal Dynamics' 01*, pp. 212–221.
- Lancaster, Peter and Kes Salkauskas (1981). "Surfaces generated by moving least squares methods". In: *Mathematics of computation* 37.155, pp. 141–158.
- Li, Tingqiu, Peter Troch, and Julien De Rouck (2004). "Wave overtopping over a sea dike". In: *Journal of Computational Physics* 198.2, pp. 686–726.
- Li, Yi et al. (2008). "A public turbulence database cluster and applications to study Lagrangian evolution of velocity increments in turbulence". In: *Journal of Turbulence* 9, N31.
- Liu, Sinuo et al. (Mar. 2019). "Viscosity-based Vorticity Correction for Turbulent SPH Fluids". In: IEEE, pp. 1048–1049. ISBN: 978-1-7281-1377-7. DOI: 10.1109/VR.2019.8798224. URL: <https://ieeexplore.ieee.org/document/8798224/>.

- Marsden, J. E. and S. Shkoller (2001). "Global well-posedness for the Lagrangian averaged Navier-Stokes (LANS- α) equations on bounded domains". In: *Philosophical Transactions of the Royal Society A: Mathematical, Physical and Engineering Sciences* 359.1784, pp. 1449–1468. ISSN: 1364503X. DOI: 10.1098/rsta.2001.0852.
- Mayrhofer, A et al. (2015). "DNS and LES of 3-D wall-bounded turbulence using smoothed particle hydrodynamics". In: *Computers & Fluids* 115, pp. 86–97.
- Mayrhofer, Arno (2014). "An investigation into wall boundary conditions and three-dimensional turbulent flows using smoothed particle hydrodynamics". The University of Manchester (United Kingdom), p. 181.
- Minion, Michael L and David L Brown (1997). "Performance of under-resolved two-dimensional incompressible flow simulations, II". In: *Journal of Computational Physics* 138.2, pp. 734–765.
- Mohseni, Kamran et al. (2003). "Numerical simulations of the Lagrangian averaged Navier-Stokes equations for homogeneous isotropic turbulence". In: *Physics of Fluids* 15.2, pp. 524–544. ISSN: 10706631. DOI: 10.1063/1.1533069.
- Monaghan, J. J. (Sept. 1992). "Smoothed particle hydrodynamics". In: *Annual Review of Astronomy and Astrophysics* 30.1, pp. 543–574. ISSN: 00664146. DOI: 10.1146/annurev.aa.30.090192.002551. URL: <http://adsabs.harvard.edu/full/1992ARA&A...30..543M>. <http://www.annualreviews.org/doi/10.1146/annurev.aa.30.090192.002551>.
- (Apr. 2002). "SPH compressible turbulence". In: 852, pp. 843–852. DOI: 10.1046/j.1365-8711.2002.05678.x. URL: <http://arxiv.org/abs/astro-ph/0204118>. <http://dx.doi.org/10.1046/j.1365-8711.2002.05678.x>.
- (2011). "A turbulence model for smoothed particle hydrodynamics". In: *European Journal of Mechanics, B/Fluids* 30 (4), pp. 360–370. ISSN: 09977546. DOI: 10.1016/j.euromechflu.2011.04.002. URL: <http://dx.doi.org/10.1016/j.euromechflu.2011.04.002>.
- (2017). "SPH- ϵ simulation of 2D turbulence driven by a moving cylinder". In: *European Journal of Mechanics, B/Fluids* 65, pp. 486–493. ISSN: 09977546. DOI: 10.1016/j.euromechflu.2017.03.011. URL: <http://dx.doi.org/10.1016/j.euromechflu.2017.03.011>.
- (1989). "On the problem of penetration in particle methods". In: *Journal of Computational physics* 82.1, pp. 1–15.
- Morris, Joseph P, Patrick J Fox, and Yi Zhu (1997). "Modeling low Reynolds number incompressible flows using SPH". In: *Journal of computational physics* 136.1, pp. 214–226.
- Muta, Abhinav and Prabhu Ramachandran (2022). *Efficient and accurate adaptive resolution for weakly-compressible SPH*. Vol. 395. Elsevier B.V., p. 115019. DOI: 10.1016/j.cma.2022.115019. arXiv: 2107.01276. URL: <https://doi.org/10.1016/j.cma.2022.115019>.
- Negi, Pawan and Prabhu Ramachandran (2022). "Techniques for second-order convergent weakly compressible smoothed particle hydrodynamics schemes without boundaries". In: *Physics of Fluids* 34.8, p. 087125. ISSN: 1070-6631. DOI: 10.1063/5.0098352. arXiv: 2107.11859.
- Negi, Pawan, Prabhu Ramachandran, and Asmelash Haftu (2020). "An improved non-reflecting outlet boundary condition for weakly-compressible SPH". In: *Computer Methods in Applied Mechanics and Engineering* 367, p. 113119.
- Nicoud, Franck et al. (2011). "Using singular values to build a subgrid-scale model for large eddy simulations". In: *Physics of fluids* 23.8, p. 085106.
- Obeidat, Anas and Stéphane P.A. Bordas (2018). "Three-dimensional remeshed smoothed particle hydrodynamics for the simulation of isotropic turbulence".

- In: *International Journal for Numerical Methods in Fluids* 86 (1), pp. 1–19. ISSN: 10970363. DOI: 10.1002/fld.4405.
- Okrashevski, Max et al. (2022). "Smoothed Particle Hydrodynamics Physically Reconsidered – The Relation to Explicit Large Eddy Simulation and the Issue of Particle Duality". In: URL: <http://arxiv.org/abs/2206.10127>.
- Panizzo, Andrea (2004). "Physical and numerical modelling of subaerial landslide generated waves". PhD thesis. PhD Thesis, Universita Degli Studi di L'Aquila, Italy.
- Pereira, Filipe S et al. (2021). "Modeling and simulation of transitional Taylor-Green vortex flow with partially averaged Navier-Stokes equations". In: *Physical Review Fluids* 6.5, p. 054611.
- Pope, SB (1994). "LAGRANGI-AN PDF METHODS FOR TURBULENT FLOWS". In: *Annu. Rev. Fluid Mech* 23, p. 63.
- Pope, Stephen B and Stephen B Pope (2000). *Turbulent flows*. Cambridge university press.
- Ramachandran, Prabhu and Kunal Puri (Dec. 2019). "Entropically damped artificial compressibility for SPH". In: *Computers and Fluids* 179, pp. 579–594. ISSN: 00457930. DOI: 10.1016/j.compfluid.2018.11.023. arXiv: 1612.05901. URL: <http://arxiv.org/abs/1612.05901%20http://dx.doi.org/10.1016/j.compfluid.2018.11.023>.
- Rennehan, Douglas (2021). "Mixing matters". In: *Monthly Notices of the Royal Astronomical Society* 506.2, pp. 2836–2852.
- ROGERS, BENEDICT D. and ROBERT A. DALRYMPLE (Apr. 2005). "SPH MODELING OF BREAKING WAVES". In: *Coastal Engineering 2004*. World Scientific Publishing Company, pp. 415–427. ISBN: 978-981-256-298-2. DOI: 10.1142/9789812701916_0032. URL: http://www.worldscientific.com/doi/abs/10.1142/9789812701916%7B%5C_%7D0032.
- Sagaut, Pierre (2002). "Statistical and Spectral Analysis of Turbulence". In: *Large Eddy Simulation for Incompressible Flows*. Springer, pp. 379–390.
- Schmitt, Francois G (2017). "Turbulence from 1870 to 1920: The birth of a noun and of a concept". In: *Comptes Rendus Mécanique* 345.9, pp. 620–626.
- Shao, Songdong (2006). "Incompressible SPH simulation of wave breaking and overtopping with turbulence modelling". In: (May 2005), pp. 597–621.
- Shao, Songdong and Hitoshi Gotoh (May 2005). "Turbulence particle models for tracking free surfaces". In: *Journal of Hydraulic Research* 43.3, pp. 276–289. ISSN: 0022-1686. DOI: 10.1080/00221680509500122. URL: <https://www.tandfonline.com/doi/full/10.1080/00221680509500122>.
- Shepard, Donald (1968). "A two-dimensional interpolation function for irregularly-spaced data". In: *Proceedings of the 1968 23rd ACM national conference*, pp. 517–524.
- Shi, Yilei et al. (2013). "Analysis of interpolation schemes for the accurate estimation of energy spectrum in Lagrangian methods". In: *Computers and Fluids* 82, pp. 122–131. ISSN: 00457930. DOI: 10.1016/j.compfluid.2013.05.003. URL: <http://dx.doi.org/10.1016/j.compfluid.2013.05.003>.
- Smagorinsky, Joseph (1963). "General circulation experiments with the primitive equations: I. The basic experiment". In: *Monthly weather review* 91.3, pp. 99–164.
- Sun, PN, A Colagrossi, et al. (2016). "Detection of Lagrangian coherent structures in the SPH framework". In: *Computer Methods in Applied Mechanics and Engineering* 305, pp. 849–868.

- Sun, PN, Andrea Colagrossi, et al. (2018). "Multi-resolution Delta-plus-SPH with tensile instability control: Towards high Reynolds number flows". In: *Computer Physics Communications* 224, pp. 63–80.
- Synolakis, Constantine Emmanuel (1986). "The runup of long waves". PhD thesis. California Institute of Technology.
- Taneda, Sadatoshi (1977). "Visual study of unsteady separated flows around bodies". In: *Progress in Aerospace Sciences* 17.4, pp. 287–348.
- VIOLEAU, D., S. PICCON, and J.-P. CHABARD (July 2002). "TWO ATTEMPTS OF TURBULENCE MODELLING IN SMOOTHED PARTICLE HYDRODYNAMICS". In: vol. 1. WORLD SCIENTIFIC, pp. 339–346. ISBN: 978-981-02-4931-1. DOI: 10.1142/9789812777591_0041. URL: http://guest.cnki.net/grid2008/brief/detailj.aspx?filename=DZDQ200901001251%5C&dbname=CPFD2010%20http://www.worldscientific.com/doi/abs/10.1142/9789812777591_0041.
- Wang, Dong and Philip L.F. Liu (2020). "An ISPH with $k - \epsilon$ closure for simulating turbulence under solitary waves". In: *Coastal Engineering* 157 (July 2019), p. 103657. ISSN: 03783839. DOI: 10.1016/j.coastaleng.2020.103657. URL: <https://doi.org/10.1016/j.coastaleng.2020.103657>.
- Yoshizawa, Akira (1986). "Statistical theory for compressible turbulent shear flows, with the application to subgrid modeling". In: *The Physics of fluids* 29.7, pp. 2152–2164.